Naval Research Laboratory

Washington, DC 20375-5320

Phase I Progress Report: Hydrodynamic Agents in the Littoral Environment

Charles M. Bachmann
C. Reid Nichols
Richard P. Mied
Ellen Bennert
Robert A. Fusina

Coastal and Ocean Remote Sensing Branch
Remote Sensing Division

Chung Hye Read

National Geospatial-Intelligence Agency
Reston, Virginia

Timothy F. Donato
Delex Systems, Inc.
Vienna, Virginia

July 6, 2007

REPORT DOCUMENTATION PAGE

Form Approved
OMB No. 0704-0188

1. REPORT DATE *(DD-MM-YYYY)*	2. REPORT TYPE	3. DATES COVERED *(From - To)*
06-07-2007	Memorandum Report	31-05-2006 to 29-12-2006

4. TITLE AND SUBTITLE		
Phase I Progress Report: Hydrodynamic Agents in the Littoral Environment		5a. CONTRACT NUMBER
		5b. GRANT NUMBER
		5c. PROGRAM ELEMENT NUMBER

6. AUTHOR(S)	5d. PROJECT NUMBER
Charles M. Bachmann, C. Reid Nichols, Richard P. Mied, Chung Hye Read,* Ellen Bennert, Robert A. Fusina, and Timothy F. Donato†	5e. TASK NUMBER
	5f. WORK UNIT NUMBER
	72-9123-A6

7. PERFORMING ORGANIZATION NAME(S) AND ADDRESS(ES)	8. PERFORMING ORGANIZATION REPORT NUMBER
Naval Research Laboratory, 4555 Overlook Avenue, SW, Washington, DC 20375-5320 Marine Information Resources Corp., Ellicott City, MD NGA, Reston, VA 20191-3449 Praxis, Inc., Washington, DC Delex, Washington, DC 22182	NRL/MR/7230--07-9056

9. SPONSORING / MONITORING AGENCY NAME(S) AND ADDRESS(ES)	10. SPONSOR / MONITOR'S ACRONYM(S)
NGA Attn: Dr. Chung Hye Read InnoVision Directorate 12310 Sunrise Valley Drive Reston, VA 20191-3449	11. SPONSOR / MONITOR'S REPORT NUMBER(S)

12. DISTRIBUTION / AVAILABILITY STATEMENT

Approved for public release; distribution is unlimited.

13. SUPPLEMENTARY NOTES

*National Geospatial-Intelligence Agency, Reston, VA 20191-3449
†Delex Systems, Inc., Vienna, VA 22182

14. ABSTRACT

Hydrodynamic Agents in the Littoral Environment (HALE) is a National Geospatial-Intelligence Agency program aimed at producing tidal predictions from imagery-derived water levels. HALE has been divided into three phases which lead to a protocol. This report describes Phase I and introduces work for Phase II. Approximately 62 satellite images of the Han River Estuary, Republic of Korea, over the 20-year period from 1987 to 2006 were processed and analyzed. The fundamental procedure involved semi-automated extraction of waterlines from high-resolution commercial imagery. Rules such as application of a red-edge index are used in quality controlling waterlines, estimating the extend of mudflats, and assessing shoreline changes due to erosion and/or sedimentation. Elevations were estimated using waterlines and a high-precision Digital Elevation Model (DEM). Elevations are determined from the intersection of the waterline with a beach profile derived from the DEM. Favorable locations have a flat gradient allowing any transects to be extended below Mean High Water (MHW). Analyses highlight the importance of shallow water tidal constituents and the utility of seasonal DEMs. Subsequent work during Phase II will focus on time series analysis involving the use of random water elevations corresponding to simulated imagery for Seward, Alaska.

15. SUBJECT TERMS

16. SECURITY CLASSIFICATION OF:			17. LIMITATION OF ABSTRACT	18. NUMBER OF PAGES	19a. NAME OF RESPONSIBLE PERSON Charles M. Bachmann
a. REPORT	b. ABSTRACT	c. THIS PAGE	UL	80	19b. TELEPHONE NUMBER *(include area code)* (202) 767-3398
Unclassified	Unclassified	Unclassified			

Standard Form 298 (Rev. 8-98)
Prescribed by ANSI Std. Z39.18

Data Disclaimer

Data and information have been synthesized to describe progress on Phase I of the Hydrodynamic Agents in the Littoral Environment project. They have not been subjected to rigorous scientific review. They are released for limited official use as preliminary data and information to be used only with appropriate caution.

PREFACE

The National Geospatial-Intelligence Agency mission involves providing timely, relevant, and accurate Geospatial Intelligence in support of national security. It does this through major facilities located in the Washington, D.C., and St. Louis, Mo., areas that are linked to liaisons and support teams stationed around the world. The InnoVision Directorate forecasts future environments, defines future needs, establishes plans to align resources, and provides technology and process solutions to lead NGA, our customers and partners into the future. InnoVision's Hydrodynamic Agents in Littoral Environment (HALE) Program is one element that is focused on linking needs, analysis, plans, advanced technologies, programs and resources to further Geospatial Intelligence (GEOINT) in the coastal zone.

HALE is aimed at improving baseline information that supports decision-making in the dynamic littoral region, and this report delineates progress made during phase 1 of this research project. HALE utilizes multi-source imagery, multi-intelligence data, and new mathematical analysis techniques to perform tide analysis utilizing imagery-derived time series of water levels. The result is a protocol to use imagery in forecasting tides so that users will know how much beach is available at all phases of the tide. Secondary benefits from this basic research improve our knowledge of hydrodynamical process across a range of tide-dominated coasts. Derived products can be used to update products such as country studies and Digital Nautical Chart. This research directly links basic research to combat support agencies.

Analysis and production are central to NGA. HALE is a multidisciplinary and integrated program that is essential to enriching GEOINT products and overcoming some of the challenges to operations along the world's coastlines, a length that has been estimated to be on the order of a million kilometers.

Chung Hye Read, Ph.D.
Program Manager
Basic & Applied Research Office
InnoVision Directorate
National Geospatial-Intelligence Agency
Reston, VA
January, 2007

iii

EXECUTIVE SUMMARY

Developing timely geospatial products through satellite feature tracking is critical for operational planning and mission execution in the coastal zone. Studies that consider imagery along with *in situ* data can establish relationships among numerous features. For example, the waterline, the interface between land and water, can be extracted from images. The waterline fluctuates in synchronization with astronomical and meteorological forces. Given a sufficient record of water level fluctuations, the waterline can be referenced to a tidal datum such as mean high water to determine the shoreline. Mean high water is derived from the average of all the high water heights over a 19-year period. In addition, long time series of remotely sensed images provide the basis to assess waterline changes, tidal flat extent and channel axes, and to estimate semidiurnal water level fluctuations along a tidal coast. Such analyses support the updating of nautical charts and development of imagery-based navigation products. Complementary field investigations and remote sensing techniques require specific data collection, analysis, and documentation phases. For this reason, the current Hydrodynamic Agents in the Littoral Environment (HALE) project is divided into three phases which lead to a protocol. This report describes Phase I and introduces work for Phase II.

This NRL Memorandum Report describes the objectives and progress made on the analysis of 66 satellite images of the Han River Estuary, Republic of Korea over the 20-year period from 1987 to 2006. Procedures involve semi-automated extraction of waterlines from high-resolution commercial imagery. Rules such as application of a red-edge index are used in quality controlling waterlines, estimating the extent of mudflats, and assessing shoreline changes due to erosion and/or sedimentation. In the next step, elevations will be determined using waterlines and a high-precision Digital Elevation Model (DEM). The waterlines serve as contours for the intertidal zone. It is already apparent from this study that the most useful DEMs should be built annually or seasonally in dynamic regions such as the Han River Estuary. Elevations are determined from the intersection of the waterline with a beach profile derived from the DEM. Favorable locations have a flat gradient and allow a transect to be extended below Mean Lower Low Water (MLLW).

Specifying the tidal elevation as a sum of the harmonic constituents, we will compute the best possible harmonic constants. This allows an analyst to estimate future water levels through harmonic prediction. Shorelines derived from this study can be referenced to the DEM's shoreline. Resulting products can be used in applications such as building an imagery-based "chartlet" for a boat company or providing baseline data for the realistic Modeling and Simulation of transition for the Expeditionary Fighting Vehicle. This phase of the study demonstrates that commercial imagery archives provide a useful tool to assemble information to understand sediment transport and predict water levels where there is no tidal reference station.

TABLE OF CONTENTS

LIST OF FIGURES

LIST OF TABLES

CONVERSION FACTORS, CONSTANTS, AND GEOGRAPHIC ESTIMATES

SI units in this Report can be converted to Non-SI units as follows:		
Multiply	**By**	**To Obtain**
millimeters	0.0394	inches
centimeters	0.0328	feet
meters	3.2894	feet
meters	0.5468	fathoms
m/s	1.9438	knots
kilometers	0.6214	miles (statute)
hectare (ha)	2.4711	acres
km^2	0.3861	mi^2 (statute)
°C	1.7999	°F – 32 °
Constants		
1 cubic foot of seawater = 64 pounds 1 cubic foot of ice = 56 pounds 1 displacement ton = 35 cubic feet of seawater Standard Time (I) = Universal Time + 9 hours		
Geographic Estimates **Areas, Volumes, and Depths**		

Water Body	Area (km^2)	Volume (km^3)	Mean Depth (m)	Greatest Depth (m)
Sea of Japan	1,007,800	1,360,530	1,350	3,742
East China Sea	1,249,200	234,850	188	2,782
Korean Straight	4,200	210+	50+	227
Yellow Sea	378,600	16,658.4	44	152
Kyunggi Bay	20,000	200	10	30

Freshwater Influence		
River	Length (km)	Drainage area (km^2)
Amnok (Yalu)	805	31,751
Tuman (Tumen)	521	24,296
Taedong	397	20,344
Han	470	26,219
Imjin	254	8,118
Yesung	174	4,048
Water Resources. Available online. URL: http://www.water.or.kr. Accessed on December 28, 2006.		

LIST OF ACRONYMS AND ABBREVIATIONS

a	tidal amplitude
A	area
AVHRR	Advanced Very High Resolution Radiometer
ASD	Analytical Spectral Devices
C	Celsius
CASI	Compact Airborne Spectrographic Imager
DEM	Digital Elevation Model
DMZ	Demilitarized Zone
DNC®	Digital Nautical Chart
EFV	Expeditionary Fighting Vehicle
F	Fahrenheit
F	formzahl
FRF	Field Research Facility
ft	feet
FTP	File Transfer Protocol
FY	Fiscal Year
GCP	Ground Control Point
GIS	Geographic Information System
GPS	Global Positioning System
HALE	Hydrodynamic Agents in the Littoral Environment
HRE	Han River Estuary
INV	tracer equation inversion
ISR	Intelligence, Surveillance, and Reconnaissance
km	kilometer
m	meter
MCC	Maximum Cross Correlation
MCIA	Marine Corps Intelligence Activity
MHW	Mean High Water
MHWN	Mean High Water Neap
MHWS	Mean High Water Spring
MLLW	Mean Lower Low Water
MSL	Mean Sea Level
NAVOCEANO	Naval Oceanographic Office
NGA	National Geospatial-Intelligence Agency
NIST	National Institute for Standards and Technology
NRL	Naval Research Laboratory
P	Tidal Prism
PAR	Photosynthetically Active Radiation
PHILLS	Portable Hyperspectral Imager for Low-Light Spectroscopy
PI	Principal Investigator
QA	Quality Assurance
QC	Quality Control

ROIs Region of Interest

second

1. Introduction

This progress report establishes the basis for deriving tide predictions from areas that are not associated with a continuous record of water level observations. For this reason, physical features such as the shoreline provide critical information to estimate water level fluctuations. This study also considers the establishment of a shoreline based on the average of 20 years of extracted waterlines. Current littoral classification systems for coastal regions are heavily slanted toward the needs of biologists and environmentalists. This report focuses on physical parameters impacting the maneuver of naval expeditionary forces. Terminology will be descriptive and highlights the environmental effects on maneuver and mission-essential tasks. This will lead to the development of a hierarchical coastal classification system that directly benefits the mapping and remote sensing community. Products will be carefully developed to support imagery, geospatial, and general intelligence analysts.

This project is being conducted in locations representative of several different coastal types. By studying the morphodynamics and tidal hydrodynamics of distinct coastal types, we will quantify the primary factors impacting strategies and tactical concepts, such as ship-to-objective maneuver, breach of the surf zone by amphibious craft, and the Expeditionary Fighting Vehicle's (EFV) transition from a planing hull to an amphibious tractor. The biological and physical features in our proposed coastal classification hierarchy are instrumental in shaping the coast as well as impacting missions. We will focus our study on temporally and spatially variable waterlines, tidal flats, water levels, and currents to determine semidiurnal, diurnal, and fortnightly tidal constituents. Analyses will highlight important information such as the transport of water through channels, the time rate of change of tidal flats, and the amount of beach that is available at all phases of the tide.

State-of-the-art software and imagery analysis techniques will be applied to define physical features of the shoreline that are associated with water level fluctuations. This will support the overall project-level goal, which is to describe the shape of the coast on a scale that is relevant to military planners and operators by accounting for the hydrodynamic processes relevant to periodic astronomical forces and meteorological forces. The final deliverable is a protocol to estimate tides based on imagery-derived water level fluctuations. Products from this research will be useful to update digital nautical charts and to build imagery-based "chartlets".

This report aims to establish descriptive terms relevant to the physical and biological processes impacting the maneuver of forces for remote sensing, mapping, and intelligence personnel. Common terms acceptable to military operators will improve the utility of state-of-the-art products that highlight highly variable environmental processes. In order to accurately describe data elements, parameters, and phenomena, a preliminary listing of terms and definitions are provided in Appendix A. Using descriptive and common names allows operators and scientists to quickly understand major biological and physical forces of importance including their magnitudes, directions, and scales of change.

1.1. Project Objectives and Scope

The initial year of the two-year Hydrodynamic Agents in the Littoral Environment (HALE) project has focused on evaluating the feasibility of extracting waterlines from imagery (*see*

Feature Analyst 4.1 for ArcGIS Training Guide) and synchronizing those waterlines with astronomically predicted tides. By comparison of imagery-derived time series of waterlines with a digital elevation model (DEM), it is possible to generate a time series of water level fluctuations at favorable locations. The waterline is analogous to a contour interval. Investigators will assess the utility of the procedure and errors that are generated by this procedure. The resultant water level time series will then be used to determine harmonic constituents of the local area. These constituents will then be used to harmonically predict tides. A protocol will be developed that helps a user build an adequate set of images and DEM's for the prediction of tides.

This research is not without difficulty. There will be systematic and random errors associated with the extraction of waterlines, the choice of a DEM referenced to Mean High Water, morphological changes at the location where water levels are obtained, data contamination by winds and spring freshets, and the use of inconsistent (random) data to harmonically analyze tides.

1.2. Work Description

The project has been divided into three phases relevant to data collection, analysis, and synthesis of information. This progress report describes the results of the first phase and provides opportunity for reviewers to help define the scope of phases two and three.

During the first phase (31 May 2006 to 29 December 2006), the focus of effort was on building a viable imagery stack from multi-source and temporally extensive commercial multi-spectral and panchromatic satellite imagery. Feature extraction software was obtained and used to derive waterlines from high-resolution commercial imagery and to convert the waterlines to shapefiles. Waterlines were quality controlled and time series of elevations were generated by comparing the waterlines to a corresponding DEM. Complementary tasks included assessing littoral features such as mudflats, determining circulation based on select image pairs, and developing a harmonic analysis procedure to determine constituents from the imagery-derived water levels.

The second phase of this project extends from 2 January 2007 to 30 March 2007. Major tasks will involve filling gaps in imagery time series to build a consistent hourly data set, applying time series analysis techniques to imagery-derived time series to estimate amplitude and phase of important tidal constituents (e.g., M_2, S_2, N_2, K_2, K_1, O_1, and P_1), and using harmonic constants to harmonically predict tides at a test site. The actual methodology is not conventional and takes the form of a seven period fit to a harmonic function. Analyses of water level time series will consider the total, tidal, and non-tidal components of the record and compare appropriate oscillations with meteorological information. Detailed comparisons will be made between predicted and observed water levels to assess the accuracy of the methodology. The residuals will be described and an error budget will be developed.

The final phase will extend from 2 April 2007 to 30 May 2007. Major tasks will involve describing the protocol for extraction of tidal constituents from multispectral data in a NRL Technical Report. All data and information will be synthesized into appendices for easy access

by operational organizations such as the Maritime Division of the National Geospatial-Intelligence Agency (NGA), the Naval Oceanographic Office (NAVOCEANO), Office of Naval Intelligence (ONI), and Marine Corps Intelligence Agency (MCIA). Digital versions of the final product will be posted on the "Enhanced Lab Environment" of NGA's Basic and Applied Research Office in the InnoVision Directorate.

2. Project Management

The HALE project was initiated by the InnoVision Directorate of NGA and is being managed by Dr. Chung Hye Read. HALE will lead to new coastal mapping technologies and shallow water process solutions. It is one component of a program that utilizes imagery to advance the knowledge base in the area of hydrodynamics. Dr. Charles Bachmann serves as the Naval Research Laboratory-Washington, D.C. (NRL-DC) Principal Investigator (PI). He is head of the Coastal Science and Interpretation Section (Code 7232) in the Coastal and Ocean Remote Sensing Branch of NRL's Remote Sensing Division.

2.1. Task Organization

There are presently five scientists from NRL-DC working on HALE with occasional support from other Remote Sensing Division scientists and colleagues from academia. One such researcher familiar with tidal forcing in the Columbia River is Dr. David A. Jay from Portland State University. As the NRL-DC PI for HALE, Dr. Charles Bachmann provides technical guidance and oversight on all aspects of HALE and reports directly to the program manager, Dr. Chung Hye Read. Key efforts by program participants include data management by Dr. Robert Fusina, feature extractions and time series analysis by Mr. Reid Nichols, data quality assurance by Ms. Ellen Bennert, and complementary feature tracking by Dr. Richard Mied.

2.2. Team Members and Responsibilities

For the current year, the HALE project has been divided into three phases. Major responsibilities for each project participant are defined in Table 2-1. The initial work is being done at the unclassified level and will become a classified project during year two. A Gantt chart is provided in Table 2-2 to illustrate some of the HALE tasks and project schedule. The project start date was 31 May 2006 and the finish date for the currently funded effort is 30 May 2007. Elements of the project include establishing a classified contract, obtaining imagery, software, a DEM, and *in situ* data, completing training, hosting technical exchange meetings, completing waterline extractions, quality controlling waterlines, building a water level time series, time series analysis, and reporting. Advancing from Phase 1 to Phase 2 was dependent on obtaining an appropriate high precision DEM and waterlines. An initial set of waterlines from commercial imagery for the Han River Estuary (HRE) have all been extracted and quality controlled. The DEM was received during the end of December, but additional collaborations with NGA are required before this product can be used. Advancing from Phase 2 to Phase 3 is dependent on successful application of time series analysis techniques to reproduce a viable tide curve from inconsistent imagery-derived elevations.

Table 2-1. Team members and responsibilities. Numerous tasks are being accomplished by the team. Members are collaborating internally as well as with interests at ONI.

Principal Investigator	Dr. Charles (Chip) Bachmann	Project oversight and funding
Project Leader	Mr. C. Reid Nichols	Coordinates data analyses (time series analysis), maintains project database, validate and assess quality of data, prepare project progress reports, and presents research results.
Co-Investigator	Dr. Richard (Rich) P. Mied	Validates and assesses quality of data, conducts least squares harmonic analysis, interprets data, and publishes research results.
Co-Investigator	Dr. Robert (Bob) A. Fusina	Assists with imagery analyses, interprets data and documents research results.
Co-Investigator	Ms. Ellen Bennert	Imagery analyses, develops project database, validates and assesses quality of data, interprets data and documents research results.

Table 2-2. Gantt chart for HALE. Percent complete indications are provided for each activity based on funding, not by technical project phases.

	Q4, FY06	Q1, FY07	Q2, FY07	Q3, FY07
TASKS				
Test Site Selection	100 %			
Image Acquisition	90 %	100 %		
Data Prep, Pre & Post-processing	90 %	95 %		
Waterline Extraction	90 %	100 %		
Development & extraction of constituents				
Demonstrate Methodology				
Validate & Document Protocol				
Apply Protocol to other locations				

■ Collection, Preparation and Processing of Commercial Imagery
■ Extraction of Tidal Constituents

3. Overview of Methodology and Resources

The initial HALE effort is a continuation of a preliminary effort by Nichols et al. (2004) to identify hydrodynamic information relevant to the HRE. Results of a literature search that supports HALE are provided in Appendix B as an annotated bibliography. We summarize remote sensing applications involving the extraction of hydrodynamic features or studies of

shorelines, mudflats, bathymetry, tidal ranges, and tidal currents. The focus is on waterlines, the line of contact between land and water. Knowing its location is important to the infantry, logisticians, sailors, and aviators. This feature is critical for planning river crossings, building bridges, erecting an elevated causeway, navigating in rivers, breaching the surf zone, and designating initial or rally points. The waterline is easily defined but difficult to map, since it is always changing. Shorelines are normally referenced to Mean High Water, a tidal datum. Such tidal datums are based on 18.6 years of consistent water level data collected at regular intervals.

Field data and imagery are complementary tools in remote sensing, especially efforts involving morphology. NGA will obtain *in situ* data and source imagery for this project. NRL-DC will be responsible for image processing, co-registration to the test sites, manual or semi-automatic extraction of waterlines, and extraction of tidal constituents. Data will be archived at NRL and available via an FTP site along with all derived products. Appendix C provides a listing of available imagery that has been used in Phase I of this project. The resolutions of imagery sources are listed in Table 3-1. For the QuickBird^{TM} imagery we have a spatial resolution in the multi-spectral bands of 4m and 15-30m for all others.

Table 3-1. Satellite sensor applications for collected images during Phase 1. The images were taken over the 20-year period from 1987 to 2006.

Satellite/ Sensor	Spectral Range (nm)	Bands	GSD	Revisit Time	Swath Width	Number of Images
ASTER	20-11650	3-VNIR 6-SWIR 5--TIR	15 m 30 m 30 m	16 days	60 km	7
Landsat	450-2080; 10420	6-VNIR 1-TIR 1-PAN	30 m 60-120 m 15 m	16 days	180 km	30
QuickBird	450-900	4-MS 1-PAN	4 m 1 m	< 3 days	8-22 km	6
SPOT	500-890	3-MS 1-PAN	20 m 10 m	7 to 26 days	60 km	23
A Ground Sampling Distance (GSD) of 10 m or less is considered high resolution.						

In the environment, phenomena are occurring at varying temporal scales from microseconds (turbulence) to millennia (climate change) and spatial scales from millimeters (entrainment) to hundreds of kilometers (sea level rise). Understanding this concept requires scientists and military planners to change from one level of detail or granularity to another in order to account for the impacts of particular phenomena. Meteorological and oceanographic occurrences, geological processes, or population movements, for example, can be examined at different granularities. This includes different spatial perspectives as well as temporal views where phenomena may be examined under real time conditions, or over hourly, daily, weekly, or longer periods. Moving back and forth among granularities is a necessary routine for what is now called, "maritime domain awareness." For this reason, an initial component of the HALE project involves quantifying the spatial and temporal scales for waterline, mudflat, and channel changes. This information will be provided in the final report and is a component of the quality control program.

HALE participants are using multi-source imagery to study shallow water processes that include variables that can be considered as data elements, parameters, and phenomena. Parameters may in some instances include two or more data elements. For example, tidal prisms are determined from imagery-derived currents and channel geometries. Such parameters are important since freshwater river discharge mixing with the influx of saltwater from the ocean may complicate tidal signals. Most estuaries are geometrically complex, and hydraulic processes and secondary circulations are tied to bathymetric features. Tides are one of the primary stirring agents that create rapidly and localized turbulent mixing. Tidal stirring is related to tidal amplitudes and numerous investigators (e.g., Parker, 1991, Boicourt, 1993, Robinson and Brink, 1998, and Jay and Kukulka, 2003) suggest that small variations in tidal amplitudes can cause large variations in mixing. Certain processes occurring over time scales of seconds and space scales of meters, such as turbulence, impact the ability of remote sensing techniques to accurately assess features from the images. Other processes such as tides occur over time scales of hours and space scales of kilometers. The propagation of the tide into an estuary is complicated by friction from complex bathymetry and river discharge. The tidal constituents of concern are called shallow-water tides (overtides) and are represented as higher harmonics of the principal lunar and solar semidiurnal constituents. Figure 3-1 illustrates the processes (dynamics) and sedimentary features (morphology) for the study sites. This effort focuses on the sediment dynamics ring of the morphodynamical corridor.

NGA is responsible for obtaining actual time series of water levels for study sites in order to assess the skill of methods. This requires coordination with hydrographic offices in several foreign countries. The preferred data is an 18.6-year record for the actual reference station that corresponds to our collection of images. Harmonic constants are also useful if actual data is unavailable. Time and height differences for secondary stations have been requested when reference station data is unavailable. In the absence of observational data a time series of predicted data for a nearby station will be used from Admiralty TotalTide (UK Hydrographic Office, 2006).

High-precision DEM's are required for this study in order to compare extracted shorelines to elevations above the DEM's shoreline referenced to Mean High Water (MHW). DEMs are created with scanned, geo-referenced topographic maps or raster images. Contour lines from the raster images are extracted, converted to digital vectors and given elevation values. Once a digital image has been fully vectorized, a raster representation of the map is created based on those vector features. If hydrographic features such as bathymetry are added to the DEM, then, prior to merging, the data must be transformed to a common reference coordinate system, both horizontally and vertically. The resolution for most DEMs can be anywhere between 5-30 meters dependent on the contour intervals on source maps. An equilibrium beach profile will be used to extend DEM elevations below MSL. According to Dean (1991) the accepted form of this profile is

$$D = Ax^{2/3}, \text{ where}$$
$$D = \text{depth}$$
$$A = \text{scale factor related to grain size, and}$$
$$x = \text{distance offshore.}$$
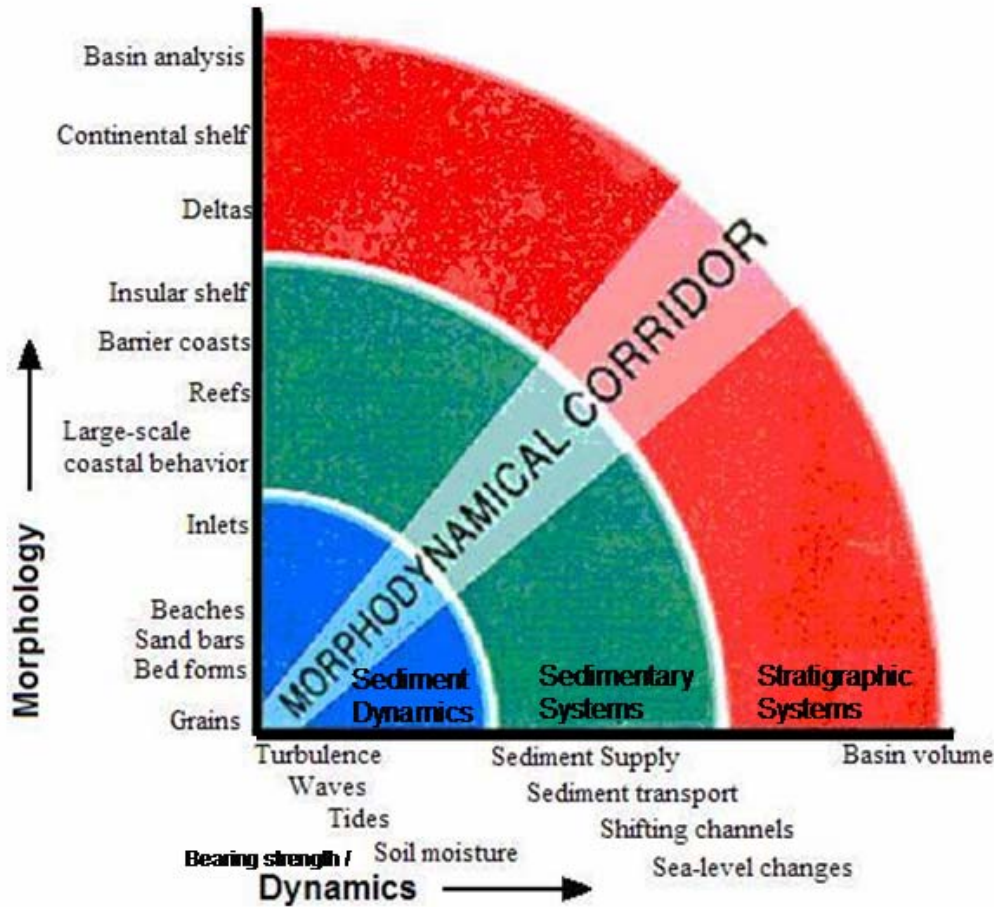
Figure 3-1. Temporal and spatial scales of coastal phenomena. At the smallest scale are the sediment particles (grains) that are transported at critical current velocities. Accumulations of clay and sand form mudflats, while erosion of sediments forms channels. These morphological features combine to form the entirety of shorelines, deltas, estuaries, and barrier islands.

The 2/3 value was determined by a survey of 500 beaches along the coast of California and Denmark. Mud tends to be composed of a combination of sand, silt, and clay. Sand grain diameters range from 0.0625 mm to 2 mm, silt particles range from 0.004 mm to .0625 mm, and clay particles are less then 0.004 mm. The scale factor value for fine sand (0.24 mm) is 0.112 $m^{1/3}$.

One task will involve building an imagery-based time series of water levels from a specific reference point. The waterlines will be intersected with a particular profile built from the DEM. The elevation is the intersection of the profile with the waterline. A separate file was built from tidal predictions near the reference point for each image. This file of predictions is used to measure the accuracy of imagery-derived elevations and as a file to initiate Phase II work. These records are provided in Appendix D.

Because the tide-generating forces are harmonic functions of time, tides themselves are essentially sinusoidal over time. For this reason, time series analysis techniques (least squares

harmonic analysis) will be used during Phase 2 of the project to develop harmonic constants. The harmonic constants consist of the amplitudes and phase relationships of the tide. These factors are reunited with the constituent tides (sums of cosine terms) in accordance with astronomical relations, for which predictions will be made. Each cosine term, or wave, will have the same period of oscillation as the astronomical forcing and we will consider at least seven cosine terms. This will be the most challenging part in the study and procedures are currently being developed. The procedure will be fully explained in ensuing reports. The process will be refined during year two.

As a transition to Phase II, information relevant to harmonic analysis is provided in Section 9 of this report. This work will focus on analysis of seven important partial tides, i.e., principal lunar (M_2), principal solar (S_2), larger lunar elliptic (N_2), and lunisolar (K_2) for semidiurnal and lunisolar (K_1), lunar (O_1), and solar (P_1) for diurnal. Of interest will be the fortnightly beat that is considered in the lunar fortnightly (Mf) and lunar monthly (Mm) constituents. Spring tides occur when M_2 and S_2 are in phase (peak at the same time) causing tides of greater range. Neap tides occur when M_2 and S_2 are 180º out of phase (are in opposition), thereby reducing tidal range. The end state will be imagery-derived curves of individual partial tides and then the total tide. We will compute the residual by subtracting predicted amplitudes from an accepted curve such as a time series of available observations. There will be a detailed analysis of the differences to determine whether they result from systematic errors, random errors, or meteorological forcing.

3.1. Laboratory Capabilities

NRL is the corporate research laboratory for the Navy and Marine Corps and conducts a broad program of scientific research, technology and advanced development. The Remote Sensing Division is specifically focused on research and development utilizing remotely sensed information or leading to remote sensing systems for applications to the earth's environment in its broadest sense.

Dr. Charles (Chip) Bachmann, as head of the Coastal Science and Interpretation Section (NRL-7232) in the Remote Sensing Division (NRL-7200), completes research related to coastal ocean surveillance, meteorological and oceanographic sensing, and operational transitions and implementations. He routinely conducts field validation studies in coastal areas having some combination of cliffs, bluffs, beaches, marshes, mudflats, and complex bathymetry. He has developed innovative feature extraction, classification, detection, data fusion, and imagery enhancement techniques.

NRL-7200 has an extensive inventory of deployable field equipment and platforms for basic research. Geophysical field equipment includes weather stations, water samplers, a gravimeter, magnetometers, wave and tide gages, data loggers, a cone penetrometer, a light weight deflectometer, and leveling and GPS equipment. The Coastal Ocean and Remote Sensing Branch (Code 7230) includes state-of-the-art sensors and growing resources of an embedded Hyperspectral Imagery Exploitation Group. Hyperspectral sensors include a CASI (Compact Airborne Spectrographic Imager) and PHILLS (Portable Hyperspectral Imager for Low-Light Spectroscopy). The Branch also maintains an extensive calibration facility using National Institute of Standards and Technology (NIST)-traceable standards. In addition, during airborne

data collection campaigns, the Branch engages in extensive field validation efforts using a suite of portable instruments including the Miniature Optical Profiler (MiniOP) and Profiling Optics Water Return (POWR) systems, 3 portable field Analytical Spectral Devices (ASD) spectrometers, an AccuPAR ceptometer, sun photometers, survey grade differential GPS equipment, and large calibration panels. NRL-7230 routinely collects quality hyperspectral datasets for research and continues to improve the calibration, atmospheric correction and geolocation before providing calibrated datasets to collaborators. NRL-7230 has also developed several software packages for exploitation of hyperspectral and other remote sensing imagery.

3.2. Hardware and Software

The HALE project is being completed with an array of high performance computer hardware and software. Computers include 7 Linux, 1 SGI, 2 Mac PCs, and 8 Windows XP. Several machines have dual processors to handle large imagery data sets and to run numerical models. The workstations are connected to several peripheral and I/O devices including a large format printer, laser printers, color ink jet plotter, and a DLT tape backup system. Workstations and printers are networked through the NRL-DC Gigabit ATM backbone. The Remote Sensing Division is completely networked with access to NIPRNET, SIPRNET, and JWICS.

A growing inventory of software in NRL-7232 (where the HALE project resides) includes 3 ArcGIS licenses, 2 Feature Analyst licenses, and 8 ENVI licenses. Various custom mathematical analysis routines are installed on workstations (using MATLAB and IDL) to include Commercial Off-The-Shelf (COTS) software for time series analysis such as single spectrum analysis (SSA). NRL-DC Code 7200 has developed specialized algorithms and processes to enable the extraction of complex features from digital imagery. These processes are typically completed with ENVI or Feature Analyst. NRL-DC has also used MIKE 3, a time domain physics-based three-dimensional model, in support of several satellite feature-tracking experiments of ocean circulation.

4. Data Modeling

4.1. Initial Resources

During the first year of this project ArcGIS 9.1 was purchased from Environmental Systems Research Institute (ESRI) and is being used as a single-user mapping and analysis tool, in the context of shoreline extractions and evaluations. Visual Learning System's software, "Feature Analyst[®]" was used as an extension to ArcGIS and is the primary image processing software to conduct multi-class feature extraction in order to define a waterline distinguishing water from land, structures, and roads. This effort could be easily expanded to a rapidly generated Geographic Information System (GIS) database and analysis plan to extract critical information for updating Digital Nautical Charts and meeting naval expeditionary warfare information requirements. Critical biological and physical information would be organized for archival storage and insertion into a hierarchical coastal classification system.

4.2. Data Model Design

A data model provides a practical template for implementing GIS projects. Building a data

model for coastal applications is one of the preliminary tasks. This data model highlights the conceptual, logical, and physical procedures that will be used to generate a geo-database derived from encyclopedic data, imagery, and *in situ* data. This data model may be adapted to initiate a GIS project ranging in objectives from updating a country study to updating a Digital Nautical Chart (DNC®). At a minimum, products and procedures will be uploaded to the Basic and Applied Research Office of NGA InnoVision Directorate's "Enhanced Lab Environment" during Phase III (Spring 2007).

The task to design and implement a coastal marine data model to extract oceanographic features such as tidal constituents is divided into four major areas. Components of the projects are illustrated in Figure 4-1. The real world requirements of our project are a necessary and sufficient quantity of commercial images of a coastal area and complementary *in situ* data from tide stations. From the imagery and meteorological and oceanographic data we can obtain data elements, parameters, and phenomena of interest. These pieces of information can be combined to comprise the conceptual area that is based on user requirements (see General Intelligence Requirements Handbook, feature and attribute codes for those needing to update maps and charts, and lists of the "Commander's Critical Information Requirements" by military units). Tasks of importance involve the definition of features and attributes, building flow diagrams on how information such as waterlines are extracted, picking GIS layers that may be updated, and ordering collections of vector based features such as

- points — soundings, navigation aids, wells, towers, and obstructions

- lines — waterlines, channels, boundaries, breakwaters and streets, and

- polygons — ponds, rice patties, mudflats, and shoals.

The major task for Phase I of this project involved the extraction of 66 waterlines from commercial imagery. There was no requirement to classify the various land category subsets associated with the interface between land and water. However, various remote sensing techniques were utilized to classify beaches, cheniers/beach ridges, tidal mudflats, marshes, and shoreline vegetation as land. A water class included rivers, flooded rice patties, ponds, and tidal channels. Challenges in multi-class feature extraction involve distinguishing between slurries, mud, sand, and remnant water from reflectance coefficients in the imagery. Section 7 explains how we accounted for these issues.

The introductory task of geo-rectifying all images and saving them into a GeoTIFF file format using ENVI® 4.2 was accomplished prior to any work with a GIS. ENVI® 4.2 was used to create a template or base image for our analysis from a high resolution QuickBird™ image. For each image, Ground Control Points (GCPs) or tie points associated with the base image were found. After locating between 10 and 15 GCPs, the image was warped and compared to the base image for consistency. The warping process re-sampled the image to the size of the base image and "tied down" the GCPs between the two images to provide the best match. When the warped image was compared to the base image, a difference of one to two pixels was considered acceptable. Once the imagery was processed, the ArcGIS® 9.1 Feature Analyst® extension was

used to execute multi-class extractions. The extracted waterline was then saved as an ESRI®
shapefile. Generating waterlines was a multi-step process where the analyst identified target
features such as land and water. The process took approximately two hours per scene since each
image was of a different quality and post processing required some manual digitizing. The work
flow is provided in Figure 4-2. It is important to emphasize that in principle an iterative approach
to refine the boundaries through the automatic classification approach would also have been
possible by re-labeling regions of residual error and re-presenting them to the Feature Analyst®
package, but a manual correction of errors was considered to be among the more rapid possible
alternatives given the current state of the Feature Analyst® machine interface.
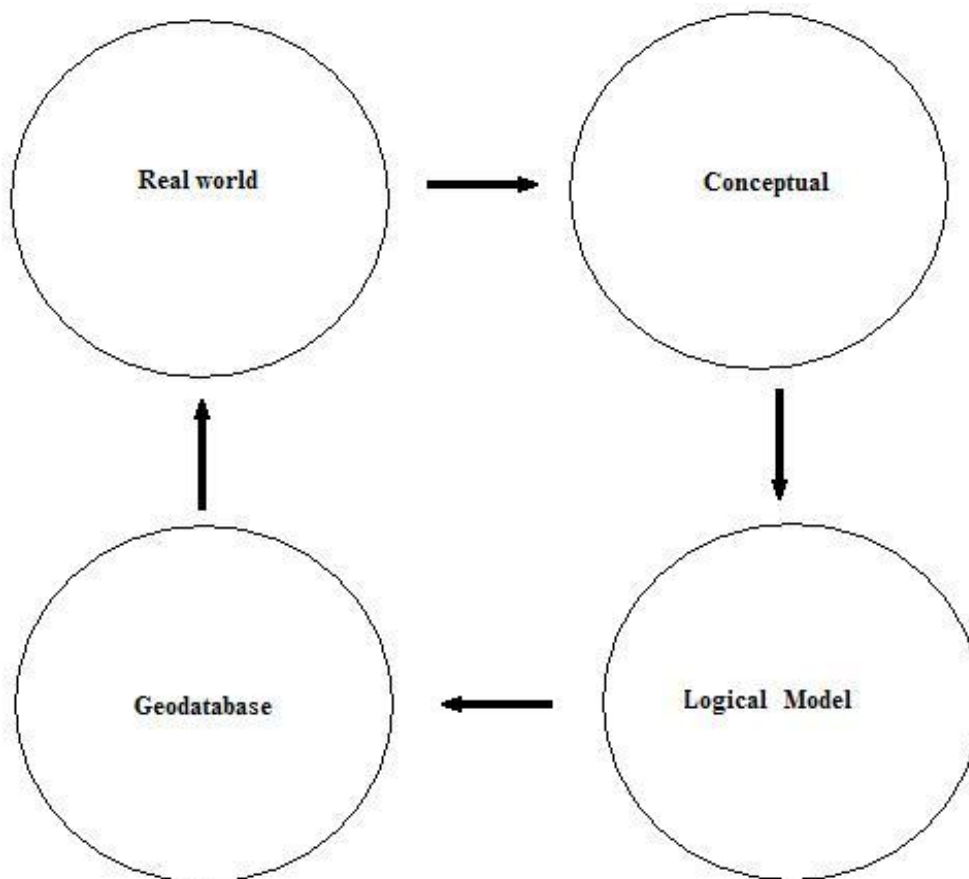
Figure 4-1. Conceptual framework for geospatial analysis. The ultimate aim is to acquire
high resolution coastal information that is committed to a geo-database for application by other
users.
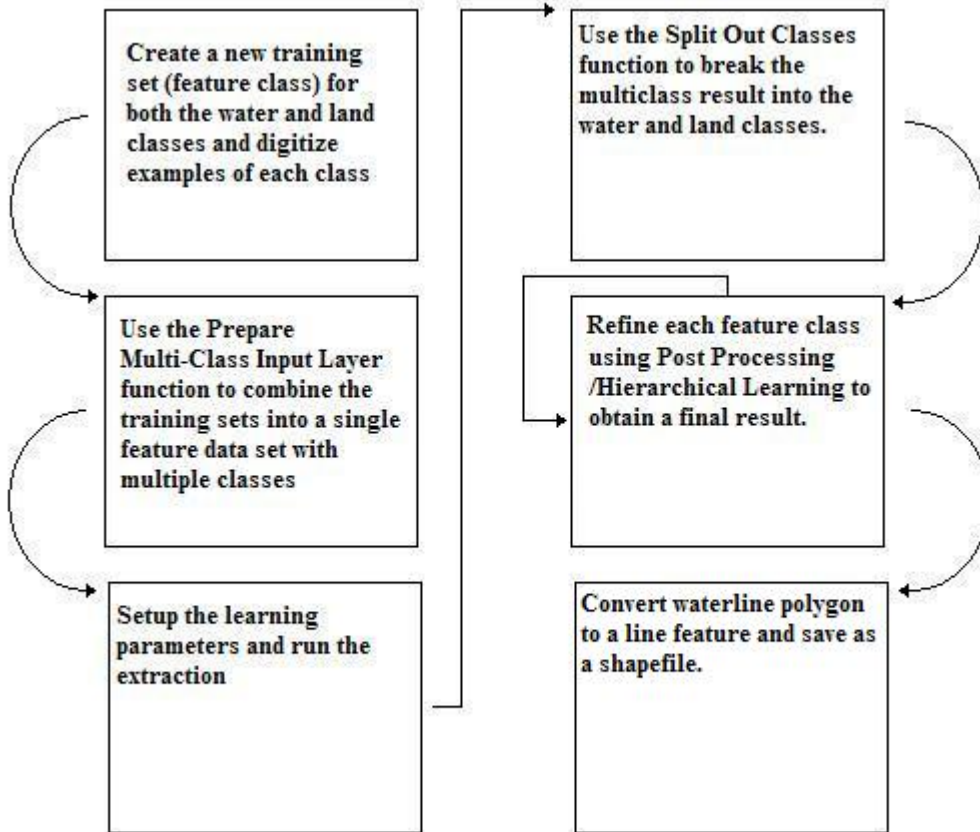
Figure 4-2. Waterline extraction workflow. The waterline method is an extremely useful remote sensing approach, especially in regions where tidal flats dominate. (Adapted from Feature Analyst® 4.1 for ArcGIS® Training Guide)

The extraction of waterlines from an imagery time series highlights changes occurring in the study area due to processes such as turbulence, sediment transport, tidal currents, tides, agriculture, and land reclamation projects. Tidal flats are characterized by low reflectance in the exposed surface due to high turbidity and variation in moisture content. There is also a remnant surface of water remaining on some tidal flats. The presence of these saturated areas may be functions of grain size, slope, and drainage. Utilizing the Maximum Cross Correlation (MCC) technique to estimate currents through channels helps to assess flooding and drying times for imagery analysts. MCC current vectors are described in Section 8 along with an alternative approach that generates somewhat more accurate results.

Once the results, such as waterlines, are extracted and quality controlled, the geographic information can be committed to a geo-database. The logical design, tabular database structure, and temporal behavior of descriptive attributes have not been determined for the HALE project. We are specifying temporal and spatial properties of data sets and archiving all information to an FTP site that is maintained by NRL-DC, Code 7200. Efforts are underway to obtain appropriate time series data for water levels and winds. A DEM for each study site is also essential.

4.3. Building a Geo-database

The use of a geo-database by NRL-DC is considered to be crucial to support other organizations such as NGA and the Naval Oceanographic Office (NAVOCEANO). Refining and updating the geo-database is an ongoing process. For example, geographic information derived from HALE may be important as links for numerical hydrodynamic and atmospheric models that rely on bathymetry or in the rapid development of an imagery-based chart. This is especially true for numerical modeling in rivers (e.g., with ADCIRC).

5. Environmental Characterization

Time series of water levels and overhead images provide a powerful tool to determine environmental forces occurring on a particular coast. Analytic software can be utilized to characterize coastal features or entities that are really dynamically changing points, lines and polygons. The associated attributes are coastal structures, waterline, channels, mudflats, and turning basins. Geographic Information Systems can then be applied to make predictions and explanations about the geographic phenomena. This report describes an initial set of waterlines that will be used to determine depths from a corresponding DEM. These imagery-derived elevations will be used to initially determine seven of the most important tidal constituents in a river-dominated estuary.

5.1. Coastal Types in General

This project will adapt the coastal classification system proposed by Shepard (1976 and 1977). These include drowned rivers, deltas, fjords, drumlins, volcanic, fault, wave erosion, barrier islands, cuspate forelands, mangroves, and coral atolls. This investigation will focus on barrier islands, wave erosion coasts, river-dominated estuarine coasts, and mangrove coasts. Relevant background materials for coast types are described in Appendix E. The coastal geomorphic classification emphasizes those physical factors that influence breaching the surf zone, crossing the beach, and movement into the hinterland. The features and attributes that are considered to have the greatest influence on mobility are:

- tidal regime (time of tide, range of tide, shape of the tidal curve),
- presence of mudflats (sediment composition, area, gradient, vegetation),
- shifting channels and shoals (length, segments, composition, depth, transport)
- beach width (composition, bearing strength, waves, slope, vegetation), and
- dune height (elevation) or obstacles (composition, maritime forest, structures).

Intelligence, Surveillance, and Reconnaissance (ISR) methods to estimate important hydrodynamic features can be optimized for each coast type. For example, finding the 6-m curve to support EFV transition may be done with acoustic sensors in turbid water associated with a deltaic coast near the Bonny River in Nigeria or using LIDAR in crystal clear waters associated with a coral coast in Indonesia. Otherwise, without a hydrographic survey, it must be estimated.

Tidal regimes can be characterized by their tidal constituents and ranges. Diurnal tides have one high and low tide per day. Semidiurnal tides have high and low tides occurring twice per

day. Mixed tides are characterized by an inequality in either the high and low water heights. For this reason, the form of the tide can be evaluated by looking at the ratio of the sums of the amplitudes of the diurnal and semidiurnal constituents. The "*formzahl*" (F) of the tide is:

$$F = \frac{K_1 + O_1}{M_2 + S_2} \text{, where}$$

K_1 = luni-solar diurnal,
O_1 = Principal lunar diurnal,
M_2 = Principal lunar, and
S_2 = Principal solar.

The following classification can be used to characterize the tide:

F: 0 – 0.25 the tide is semidiurnal,
F: 0.25 – 1.5, mixed mainly semidiurnal,
F: 1.5-3.0 mixed mainly diurnal, and
F: 3 - ∞ diurnal.

Tidal ranges may also be averaged in order to categorize tidal energy based on the geographic region. Tidal ranges between 0 - 2 meters are classified as micro-tidal. Example areas include the coastal zone between Cape Hatteras, NC and Bull Bay, NC. Tidal ranges between 2 - 4 meters are classified as meso-tidal such as the coast zone between Bull Bay, NC and Savannah, GA. Tidal ranges greater than 4 meters are classified as macro-tidal such as the Bay of Fundy in Canada or along portions of the west coast of Korea near the HRE.

The extensive stack of HALE images provides an opportunity to study features such as mudflats, which can be broken down into sections and characterized by gradients, widths, and channel flows. One task associated with the quality control of extracted waterlines involves assessing changes and trends in mudflat attributes. This result provides an important context to assess current and potential channel conditions that may be represented in an updated nautical chart. An important task for this project is the determination of a stable location that can be used as an imagery-derived reference station to build a time series of water level fluctuations.

Estuaries with extensive connecting channels and mudflats may have a strong tidal signal. Remote sensing provides the spatial coverage to characterize water flow and assess channel stability, which helps to predict locations where there may be scour or the development of bars. Changes in the location and extent over time are indicative of differences in water discharge or sediment transport capacity. Therefore, one might determine the maximum tidal flow discharge per unit width as a function of the water depth. For example, the volume of water that enters through a channel during flood flow and then exits during ebb flow is known as the tidal prism. Tidal prism (P) may be estimated as the area of the estuary times the magnitude of the water level increase in the estuary during flood tide,

$P = 2\, a_e\, A_e$, where
a_e = tidal amplitude in the estuary, and
A_e = estuary area.

14

Another useful measure involves the computation of discharge through channels. As mentioned earlier, applying the MCC method between sequences of images and multiplying current speeds by the cross-sectional area provides an estimate of volumetric flow. Such techniques help to characterize the different sections of a mudflat and segments of a channel.

Mudflats will vary in extent based on the tidal regime and water flow. In estuarine coasts water flow is principally a function of hydraulic currents and tidal currents. Hydraulic currents are forced by differential pressure heads and rectilinear tidal currents are driven by the astronomical forces. As the flow from rivers enters larger bodies of water, its velocity slows. Sediment transported by the river will then be deposited with more coarse material falling out first and the finer grains, silt, and clays settling further out in the water body. Similar to the mudflats, channels will shift as a consequence of composition and flow patterns. Flow may be impacted by anthropogenic factors such as land reclamation.

A very important attribute for characterizing the shoreline will be the extent to which beach width changes in response to tides, winds, waves, flooding, etc. The shape of beaches over time is influenced by storm events (days), normal seasonal changes in wave intensity (month to year), and longer-term events such as hurricane activity, El Niño, and climate change (years to centuries). The character and form of the beach is the result of processes such as erosion and accretion. Other shore forms include cliffs, bluffs, and marshes.

Dunes, breakwaters, groins, and bulkheads may protect the beach. These natural and man-made shore protection structures will be categorized based on their impact on the maneuverability of hovercraft, tracked vehicles, and wheeled vehicles.

5.2. Selected Coastal Types for Analysis

Physical and biological features may be categorized into a hierarchical system in order to make a coastal classification. The particular coast could fit several classes, but falls into one category or another based on objective considerations such as primary sediments, beach composition, wave climate, climate, vegetation, tide type, shoreline configuration, rates of erosion, and surf. This two-year study will assess spatially and temporally varying processes occurring in barrier island, wave erosion, estuarine, and mangrove coasts.

Barrier island coasts are dominated by long linear islands that parallel the mainland. These islands may contain salt marshes, maritime forests, and dune fields. They are composed of mud along tidal flats which face an estuary and sand- to gravel-sized sediment facing the sea. The estuary separates the barrier island from the mainland. Depending on physical processes such as depth, evaporation, and circulation, the estuaries may exhibit particular geophysical characteristics that allow them to be classified as bays or lagoons. River mouths and tidal inlets connect these estuaries to the coastal ocean. Owing to a gently sloping continental shelf, barrier islands are common to the east coast of the United States. They form in response to winds and wave dominated or mixed energy environments. They tend to be associated with micro-tidal or meso-tidal regimes. Prevailing winds can build a mound of water or "pressure head" on one side of a tidal inlet leading to exaggerated ebb and flood currents. These hydraulic currents may

persist beyond the predicted times and durations for ebb, slack, and flood tidal current conditions.

Wave erosion coasts develop in response to wind, waves, and currents, which erode the adjacent land. The interaction of water, wind, and land is the cause of erosion. On elevated coasts with headlands and promontories, wave processes transform the promontory into sea cliffs, caves, arches, stacks, and tombolos. As the sea cliff retreats, eroded material forms wave-cut terraces where wave energy is dissipated. The terraces reduce wave attacks upon the cliffs. Continued processes associated with cliff erosion include slope failure, landslides, block falls, debris slides, and cave collapses.

There are many locations where rivers and oceans meet, such as in bays and bights. In an estuarine coast there is a partially enclosed coastal body of water where saltwater is measurably diluted by freshwater from land drainage. Marines and Sailors are particularly concerned with features relevant to navigation such as length, width, and depth of channels (boat lanes) as well as the associated waves, tides, and currents. This study will focus on river-dominated, coastal lagoon, and fjord type estuaries. Follow on work may take place at the Virginia Coast Reserve, which is near the mouth of the Chesapeake Bay.

Mangrove trees are generally found on coastlines between 25° N and 25° S latitude and are affected by air temperature, salinity, and storms. Red mangroves are more cold tolerant. Black mangroves can tolerate very high salinity and very anoxic conditions. White mangrove trees have an affinity for lower salinity areas. All species need gentle wave/tidal action to bring nutrients. Consequently, mangrove coasts are associated with extensive mangrove forests that fringe shorelines, canals, rivers and lagoons. Mangrove coasts may also be associated with offshore coral reefs.

5.3. Beach Types

For this project, waterlines are the instantaneous land-water boundary at the time of the imaging process. Shore forms that will be observed on imagery include beaches, cliffs, and marshes. As part of building metadata for the extracted waterlines, shore forms such as beaches and marshes will be described. In addition finding a stable beach that is in balance between erosion and accretion will be useful in studying water level fluctuations. A stable beach is paramount to selecting a reference for imagery derived tide predictions.

Beach changes are caused by seasons, storms, and coastal construction. Beach shape is also dependent on composition and the physical processes (waves, tides, ice) impacting the unconsolidated sediments. The shape and the significance may also vary in accordance with scale. Every beach is unique and develops from its own source and type of sediment. For example, beaches in Hawaii may consist of "black sand" derived from the erosion of volcanic rocks, "white sand" made by the shells of marine organisms, or a mixture of both. Barrier island beaches along the east coast of the United States are composed of quartz sand derived from the weathering of continental rocks. Mudflats common to the west coast of the Korean peninsula are a combination of silt and sand.

For military applications, beaches may be classified according to their shape and vertical gradients. Spatial scales and shape will impact integrated beach defenses, maneuver, and the logical location of primary and alternate fighting positions as well as avenues of approach. In this context, landing beaches are generally long and straight, convex such as a peninsula or point, or concave, such as a pocket beach. Length scales are on the order of kilometers as opposed to long stretches of coastlines and bights (concave) that have length scales on the order of 100s of kilometers. Beach gradients contribute to the manner in which waves break as surf (spilling, plunging, collapsing, and surging), which impacts the ship to shore maneuver for amphibious craft and vehicles.

Beach forms may also be classified based on composition and compaction of materials. From grain sizes and the shear strengths of the beach, analysts can determine gradients and trafficability. Muds and fine grains (< 250 µm) are associated with low energy beaches and gentle gradients. Coarse sand, gravel and cobble (> 1 mm) are associated with high-energy beaches and steeper gradients. Classifying the beach according to the relative strength of the sediments supports the development of trafficability maps to locate cushion landing zones and exits of the beach.

5.4. Surrogate Environments

Navy and Marine Corps Bases are used to develop, organize, equip, train, administer, manage, logistically support, and otherwise prepare units to accomplish assigned missions. Major training areas do not offer ideal locations to acclimatize Marines and Sailors for world-wide deployments sites. For this reason pre-deployment training exercises such as Joint Task Force Exercises and Certification Exercises are often planned and executed at various sites around the country or use "synthetic geography" and well-crafted master scenario event lists. Exercise designers often attempt to insert natural disasters into the exercise using scripts.

A coastal classification system provides planners with an authoritative hierarchical system defining physical and biological factors that shape the battlefield. Planners can evaluate the suitability of training areas to meet the challenges common to the area where they will be operating. In addition, training simulations can be developed to provide authoritative representations of the coastal zone that are based on an accepted classification system. This is a first step toward creating a surrogate environment, where the effects of coastal type on weapon systems can be examined. This could be applied to most modeling and simulation tools. It would force commanders to change from one level of granularity to another when considering the impacts of hydrodynamic agents on mission success. It would also support simulation based acquisitions.

Military bases such as Camp Lejeune provide centrally managed geospatial databases containing hundreds of layers of geographic information, imagery sets, engineering drawings, photographs, and links to external databases. These provide a basis to develop custom products such as special maps for training that may even contain synthetic geography, geology, and meteorology to add realism in training. Marines and Sailors could be given authoritative ISR products as "geospatial value-add" to build their own products in preparation for deployments to various other coast types having very different climatological backgrounds.

6. HALE Project Locations

Test sites include micro- (tidal range = 0-2 m), meso- (tidal range = 2-4m), and macro-tidal (tidal range > 4m) regions. A brief description is provided to characterize each site that was selected by the National Geospatial-Intelligence Agency (NGA). After looking at initial data and available imagery, the macro-tidal HRE was selected as the best location to develop a protocol for the extraction of tidal constituents from commercial imagery.   The HRE geography and hydrodynamics are described in Section 7, Problem Definition and Example Application.

6.1. Duck, North Carolina

A resort town that is located on the northern portion of the Outer Banks. This site allows opportunity to pull data and information from the U.S. Army Corps of Engineer's Field Research Facility (FRF), an internationally recognized coastal observatory. Instruments at the facility constantly record the changing waves, winds, tides, and currents from a pier that extends approximately 560 m across the surf zone and into the offshore area. The barrier island separates the Atlantic Ocean from Currituck Sound. The closest inlet to the FRF is Oregon Inlet to the south. Tidal ranges for this micro-tidal site are provided in Table 6-1.

Table 6-1. Duck Pier is a secondary harmonic port. The tide type is semidiurnal.

Highest High Water	MHWS	1.1 m
Lowest High Water	MHWN	0.9 m
Mean Sea Level	MSL	0.54 m
Highest Low Water	MLWN	0.1 m
Lowest Low Water	MLWS	0.0 m

Duck, NC represents a barrier island coast. These long, narrow, offshore deposits of sand are common to the United States' Atlantic and Gulf of Mexico seaboard. They include a beach, dune, barrier flat, and salt marsh. The beach at the FRF is straight.

6.2. Everett, Washington

The Snohomish River begins at the confluence of the Skykomish and Snoqualmie rivers and empties into Everett Harbor and then Possession Sound. At its lower end, the Snohomish flows through a wide valley bounded by morainal deposits. About 12 km upstream from Possession Sound, at an elevation of less than 1.5 m above sea level, the main channel divides into several distributaries, i.e., Ebey Slough, Union Slough and Steamboat Slough. Spring-tide range in the sloughs is as much as 5 m. Most of the river is edged with either forest or farm. The Snohomish River has formed a tidal flat of about ten square miles in area. During extreme low tides, much of this area is exposed, and the river moves westward to Possession Sound through channels cut by the sloughs, and south to Port Gardner Bay through the dredged main channel. The Snohomish delta consists of subtidal channels, intertidal flats and point bars, marsh, and lower delta plain and levees. Tidal ranges for this meso-tidal site are provided in Table 6-2.

Everett, Washington provides an estuarine coast where the Snohomish River mixes with salt water from Possession Sound. Possession Sound is part of the flooded glacial valleys

comprising the Puget Sound fjord system. Mudflats and dredged channels extend along the man-made Jetty Island.

Table 6-2. Everett is a secondary harmonic port. The tide type is diurnal.

Highest High Water	MHHW	3.2 m
Lowest High Water	MLHW	3.0 m
Mean Sea Level	MSL	1.99 m
Highest Low Water	MHLW	1.8 m
Lowest Low Water	MLLW	0.0 m

6.3. Kings Bay, Georgia

Kings Bay is located on the western shore of Cumberland Sound, a protected bay behind Cumberland Island. Cumberland Sound is connected to the Atlantic Ocean through a dredged inlet channel called St. Mary's Entrance. The inlet is protected by two jetties separating Cumberland Island, Georgia, to the north from Amelia Island, Florida, to the south. Cumberland Island is a barrier island off the coast of Georgia just north of the Florida border. Barrier islands are dynamic habitats resulting from geologic interactions driven by sea level rise, wave-driven erosion, accretion, and overwash processes caused by storms. The ocean side of Cumberland Island is characterized by wide sandy beaches, beyond which lie primary and secondary dunes with lower interdunal areas. On the back side (west) of the island is a broad expanse of salt marshes and tidal creeks. These marshes, which eventually feed into Cumberland Sound, serve to separate the island from the mainland. Tides, which are semidiurnal, can exceed 2.1 m during spring tide and are approximately 1.8 m at neap tide. Tidal ranges for this meso-tidal site are provided in Table 6-3.

Table 6-3. Kings Bay (Cumberland Sound) is a secondary harmonic port. The tide type is semidiurnal.

Highest High Water	MHWS	2.1 m
Lowest High Water	MHWN	1.8 m
Mean Sea Level	MSL	1.05 m
Highest Low Water	MLWN	0.2 m
Lowest Low Water	MLWS	0.1 m

Kings Bay provides a coastal lagoon estuary dominated by the St. Mary's River, the principal tributary of Cumberland Sound.

6.4. Freetown, Sierra Leone

Apart from the mountainous Sierra Leone (Freetown) Peninsula some 45 km long at the mouth of the Rokel River, the coastal zone is flat with fringing mangrove swamps that extend 30 km inland. Besides mangrove swamps, there are a number of depositional and erosional features such as sandy beaches, spits, cliffs, lagoons, and estuaries. Tides are semidiurnal and the mean spring tide range at Freetown is 3 m. Tidal ranges for this meso-tidal site are provided in Table 6-4.

Table 6-4. FREETOWN is a standard harmonic port.

Highest High Water	MHWS	3.0 m
Lowest High Water	MHWN	2.3 m
Mean Sea Level	MSL	1.77 m
Highest Low Water	MLWN	1.0 m
Lowest Low Water	MLWS	0.4 m

This is a semidiurnal location. Other than the mountainous Sierra Leone Peninsula (Freetown), the sheltered coast is dominated by mangroves and mudflats. However, for this study the chosen area includes the estuary dominated by the Sierra Leone River, which divides into Port Loko Creek and Rokel River. Shoreforms include rocky headlands, low cliffs, and pocket beaches.

7. Problem Definition and Example Application

The Han River Estuary (HRE) is an excellent site to experiment with the extraction of waterlines from imagery and to analyze hydrodynamic features such as water level fluctuations, sediment transport, and coastal erosion. The west coast of Korea is the location of some of the most extensive tidal flats in the world and has extremely large tidal ranges. The Han River, which meanders through Seoul, is also one of the major Korean rivers emptying into the Yellow Sea. Figure 7-1 provides the geography of the study area from a current DNC®, Volume number DNC23ED17. The DNC® is produced by NGA as a vector-based, digital database containing significant maritime features essential for safe marine navigation.

Extracted waterlines highlight the border between land and sea, which is hard to detect in a region dominated by mudflats. As indicated in Figure 7-2, the boundary consists of intertidal sand shoals, cheniers/beach ridges, and tidal channels. A shoreline is the boundary between land and water, referenced to the tidal datum such as mean high water. In the absence of such a datum, this investigation will assess the accuracy of waterline products derived from some subset of 66 imagery-derived waterlines. A DEM, referenced to mean sea level, will be used to determine elevations from known points. These elevations will then be used to estimate harmonic constants for tide predictions.

7.1. Remote Sensing and Hydrodynamic Challenges

The coast type presents certain generalized features owing to common forces shaping all coasts. Waves, tides, and currents are responsible for carrying and flushing sediment perpendicular to the coast while wave-driven littoral transport (longshore drift) and the Coriolis force moves and redistributes sediment parallel to the coast.

In micro-tidal coasts, features such as barrier islands may be tens of kilometers long with occasional tidal inlets. Because of the dominant littoral currents, inlets formed during storms rarely remain open, but rapidly migrate in the direction of the longshore drift and fill. Inlets between barrier islands on meso-tidal coasts are more abundant because of the increased flushing capacity of the tides. The large amount of sediment that is carried through the inlet is deposited

on both the seaward (ebb tidal delta) and shoreward (flood tidal delta) side. As flood tidal deltas build up they develop into vegetated marshlands. Macro-tidal regions tend to be associated with funnel-shaped embayments with offshore linear sand bars and broad marginal tidal flats.

Our initial effort endeavors to determine tidal constituents remotely through the use of overhead sensors in a macro-tidal coast. Methodologies are being developed for validation at test sites that represent various coast types within the continental United States; these coastal types are representative of those found throughout the world. However, the test site for the initial year of this study is the HRE since it is a region of strategic interest, has an extremely large tidal range, and provides hydrodynamic challenges relevant to sediment transport.

Follow-on efforts will apply the developing technique in meso- and micro-tidal regions mentioned in Section 6. Imagery and tidal hydrodynamic background information has been collected for the HRE and may complement studies being conducted by other researchers concerned with the morphology of mudflats.

7.2. Application

HALE is using multi-source imagery to develop a GIS database that helps analyze information common to coastal regions. A feature dataset is currently being generated for an approximately 250 km^2 region that includes the HRE. Extracted attributes emphasize dynamically changing features such as waterlines and mudflats. Attributes contain more information than just name, length, and average depth. We are computing shoreline retreat rates, channel areas, channel segments, and discharge. The extractions are available for use in updating products such as DNC$^®$ or in building imagery-based "chartlets".

7.2.1. Geographic Background

Korea is a 1,000 km north-south trending peninsula separating the Yellow Sea from the Sea of Japan. The T'aebaek mountains in South Korea and Nangnim mountains in North Korea, form the north-to-south backbone of the Peninsula and the drainage divide between the western and eastern slopes. There are some substantial limestone cave systems in both North and South Korea. There are no glaciers, active volcanoes, or strong earthquakes. The rural population is focused on agriculture that is concentrated along the plains, low hills, and riverine areas common to the west and south coasts. The east coast has no significant plains or rivers, since mountain slopes generally rise directly from the shoreline. The western coast is highly indented with islands and estuaries, while the east coast is generally smooth with no islands.
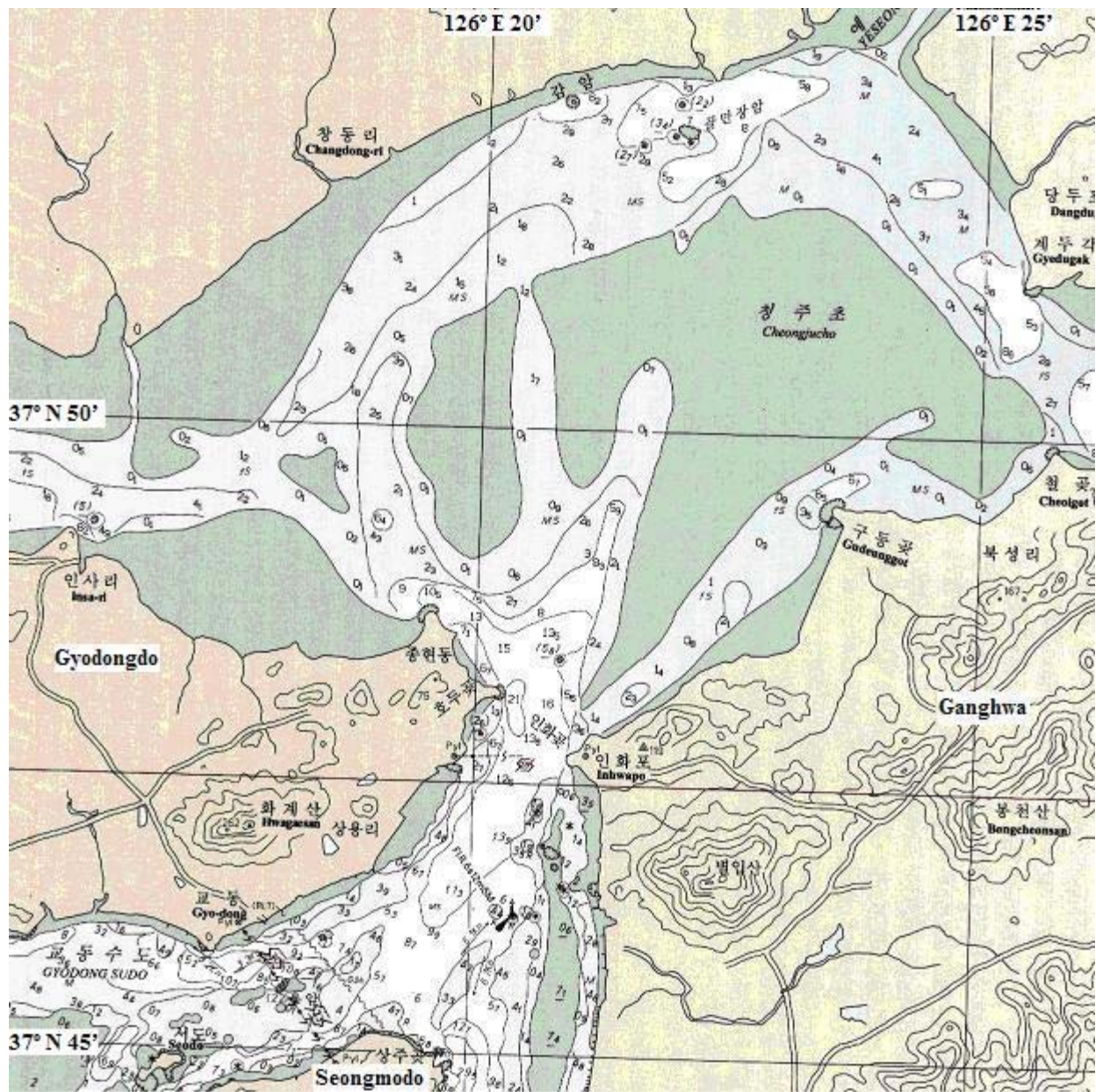
Figure 7-1. Geography of the HRE. This graphic was obtained from NGA's DNC®, Volume number DNC23ED17. This "chartlet" depicts the northeastern tip of Gyodongdo Island and the northwestern tip of Ganghwa Island. The northern peninsula of Seongomodo Island is located to the south. The Yesung River is located to the north and the Han River enters from the east after passing through the Seoul metropolitan area. The Gyodong waterway is between Seongomodo and Gyodongdo Islands.

Figure 7-2. Korean mudflat. This Gyodongdo Island mudflat is located near the mouth of the Han River and was imaged by the QuickBird^{TM} satellite at low tide on 28 April 2006. The image shows two concave beaches, mudflats, sandy beaches, rice paddies, and promontories.

Korea's rivers flow into the Yellow and East China Sea after draining the western and southern slopes of the Peninsula. The land boundary between China and Korea is largely formed by two rivers: the Amnokkang River (Yalu River in Chinese) and the Tuman River (Tumen River in Chinese). The last 16 kilometers of the Tuman River also serve as a boundary with Russia. The Amnokkang River flowing 800 km southwest empties into the Yellow Sea; the Tuman River first flows northeast and then southeast for 500 km before emptying into the Sea of Japan. The Han River is approximately 470 km-long with its basin measuring 26,219 km^2. It covers extensive regions of the middle part of the Peninsula, including Gangwon-do, Chungcheongbuk-do, and the Gyeonggi-do provinces. The Kum River is approximately 401 km long and empties into the Yellow Sea at Kunsan. The Naktong River flows south for approximately 523 km from the T'aebaek Mountains and enters the Korean Strait near Busan.

The western and southern coasts are very irregular with islands, small peninsulas, bays, and small beaches composed of sand and gravel. A broad estuary is formed where the Imjin River flows into the Han River. The Imjin River is approximately 254 km in length and floods under the influence of monsoon rains during the summer. Plains along the west coast are important rice-producing regions. The Han River plain near Seoul is one of the most extensive (MCIA, 2000). Many rice fields depend on rivers for irrigation and dams are found along most of

the rivers. The west coast, facing the Yellow Sea, has a macro-tidal tidal range and is associated with a shallow continental shelf. Tidal flats composed of mud are extensive, especially near the river mouths and between islands where there is sheltering. Mudflats are reportedly from 5 to 25 m thick (Bird and Schwartz, 1985 and Choi et al., 2004). The water is very turbid. Tidal flats are under extensive reclamation for agricultural land and salt pans.

Tidal fluctuations along the mudflats of the HRE can significantly alter the distance to shore and may render long stretches of coastline inaccessible for hours at a time. Tables 7-1 and 7-2 provide tidal ranges for the region near the HRE. As an interesting historical point, U.S. forces executed a surprise landing during high tide at Inchon, Korea during 1950. The amphibious assault would have been impossible during low tide due to extensive mudflats.

There are many Islands located near the HRE and some are Ganghwa, Seokmodo, Jumundo, Boleumdo, and Gyodongdo. To the north of Ganghwa Island and across the Han River is Kaesŏng (Gaeseong), North Korea.

Table 7-1. TotalTide Station Number 7480 located at Oep'ori. This is a secondary harmonic port located at 37º 42' N; 126º 22' E. The tide type is semidiurnal.

Highest High Water	MHWS	8.2 m
Lowest High Water	MHWN	6.0 m
Mean Sea Level	MSL	4.57 m
Highest Low Water	MLWN	3.1 m
Lowest Low Water	MLWS	1.0 m

Table 7-2. TotalTide Station Number 7486 at Inchon (formerly Chemulpho). This is a standard harmonic port located at 37º 28' N; 126º 36' E. The tide type is semidiurnal.

Highest High Water	MHWS	8.5 m
Lowest High Water	MHWN	6.4 m
Mean Sea Level	MSL	4.64 m
Highest Low Water	MLWN	2.9 m
Lowest Low Water	MLWS	0.4 m

7.2.2. Climatic Summary

South Korea has a humid, East Asian monsoonal climate. Winter temperatures are often below freezing (winter temperatures in Seoul average 3.5º C) while summers are hot (summer temperatures in Seoul average 25.3º C). The temperature range between the coldest (February) and hottest (August) months is about 21.8º C in Seoul. The cold winters are due in part from a continental high pressure system over Siberia which blows dry, cold northwesterly winds into Korea. Water temperatures lag air temperatures and many rivers freeze in Korea during the winter. Springs bring precipitation and temperatures are mild. Summer is associated with monsoon rains (June to September), which cause some rivers and streams to flood. Park et al. (2002), report that freshwater discharges from the Han, Imjin and Yesung Rivers are on the order of 315, 100, and 50 m^3s^{-1}, respectively.

The HRE study site includes a water area of approximately 120 km^2 and is sheltered from ocean swell by islands. The maximum fetch is approximately 17 km from the southwest (Kyodong waterway) to the northeast (Yesung River) direction. The shortest cross-basin axis is 9 km. Extensive mudflats have developed in part due to the high tide range that is approximately 3 and 8 m during periods of neap and spring tides.

7.2.3. HRE Problem and Task Descriptions

Remote sensing analysis and GIS work is being accomplished as described in Section 6. Scenes clearly identify regions of land and water. Discrimination between the two is slightly more complex in mudflat regions, especially when there are edge match issues. At times there are multiple pixels along the edge whose values do not match. The waterline position can be best located when using a mid-infrared channel. Manual extractions based on visual interpretation must be used to edit waterlines, especially for panchromatic images. Waterlines were extracted from 66 multi-source images, which did not lend itself to batch processing with feature extraction software. The waterline is the observed land-water interface from the satellite image. Since the waterlines fluctuate with rising and falling tide, they are compared to a DEM to determine water level fluctuations at an imagery-based reference point. ArcGIS® 9.1 is being used as the project GIS, i.e. as a single user mapping and analysis tool.

7.2.4. Waterline Extraction

Generating the waterline extraction is multi-step process that utilized Feature Analyst® 4.1 for ArcGIS®. The multi-class extraction involved digitizing training examples of water and land classes as shown in Figure 7-3.
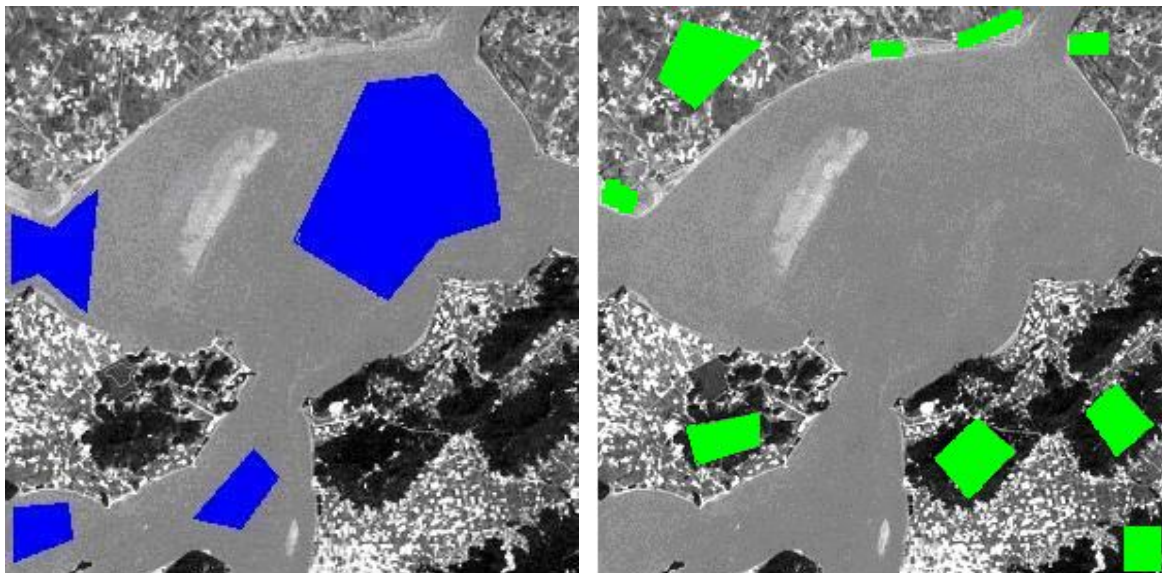
Figure 7-3. Multi-class shapefiles. Water (left panel) and land (right panel) are digitized and saved as a shapefile. The Landsat image was taken at the beginning of an ebb cycle on 23 September 2001.

After water and land classes have been created they are combined into a single multi-class layer.

Feature Analyst® used the water and land polygons or training targets for feature extraction. For this reason, it was important, especially with panchromatic images, to provide detailed examples of mudflat features that needed to be extracted. This was accomplished by zooming into the frame to characterize beaches and exposed shoals as land polygons. On some panchromatic images a histogram stretch was applied to increase contrast and to build a texture file. This served as a "texture" band for the analysis of panchromatic images. After a Feature Analyst extraction was run on the image to produce a multi-class results shapefile, the "split out class" option was used to separate the polygon water class from the multi-class results. The boundary of the polygon water class was then saved as the waterline shapefile. An example that includes the result and a post processed shoreline is provided in Figure 7-4.

Feature Analyst® provides various tools to post process shapefiles that range from de-cluttering and aggregating polygons to smoothing edges. In addition, sections of coastline can be cut and modified based on visual interpretation. Although not a mathematical tool, *post facto* hand editing provided a quick and reliable edge-detection method. In some cases, clouds were observed in images and adjacent shorelines were used to interpolate the missing data. We have currently extracted 66 waterlines that are shown graphically in Figure 7-5.

7.2.5. Quality Control Procedures

As of this writing, Quality Control (QC) procedures were performed only on HRE imagery, though they are applicable to data from any location. Each satellite image, along with the corresponding waterline data, is inspected. The locations and areas of noteworthy features are recorded and a metadata document is created. This includes channels, segments, mudflats, and the identification of several key point and linear features that may be used as a reference.

The first step in the process is the visual inspection (Figure 7-6). Each image is opened with the ENVI® software package, one at a time. ENVI® has an "Overlay" feature which can be used to add latitude and longitude grid lines as well as the waterlines from the Feature Analyst shapefile. The grid lines can be modified and the most convenient intervals to use were 2'15" (0.0375°). The waterlines are inspected first. Any place where the lines are found to be too far on either side of the visual boundary is noted so that additional post processing can be accomplished. Any interesting features found in the image, such as clouds or especially turbid plumes, are also noted.
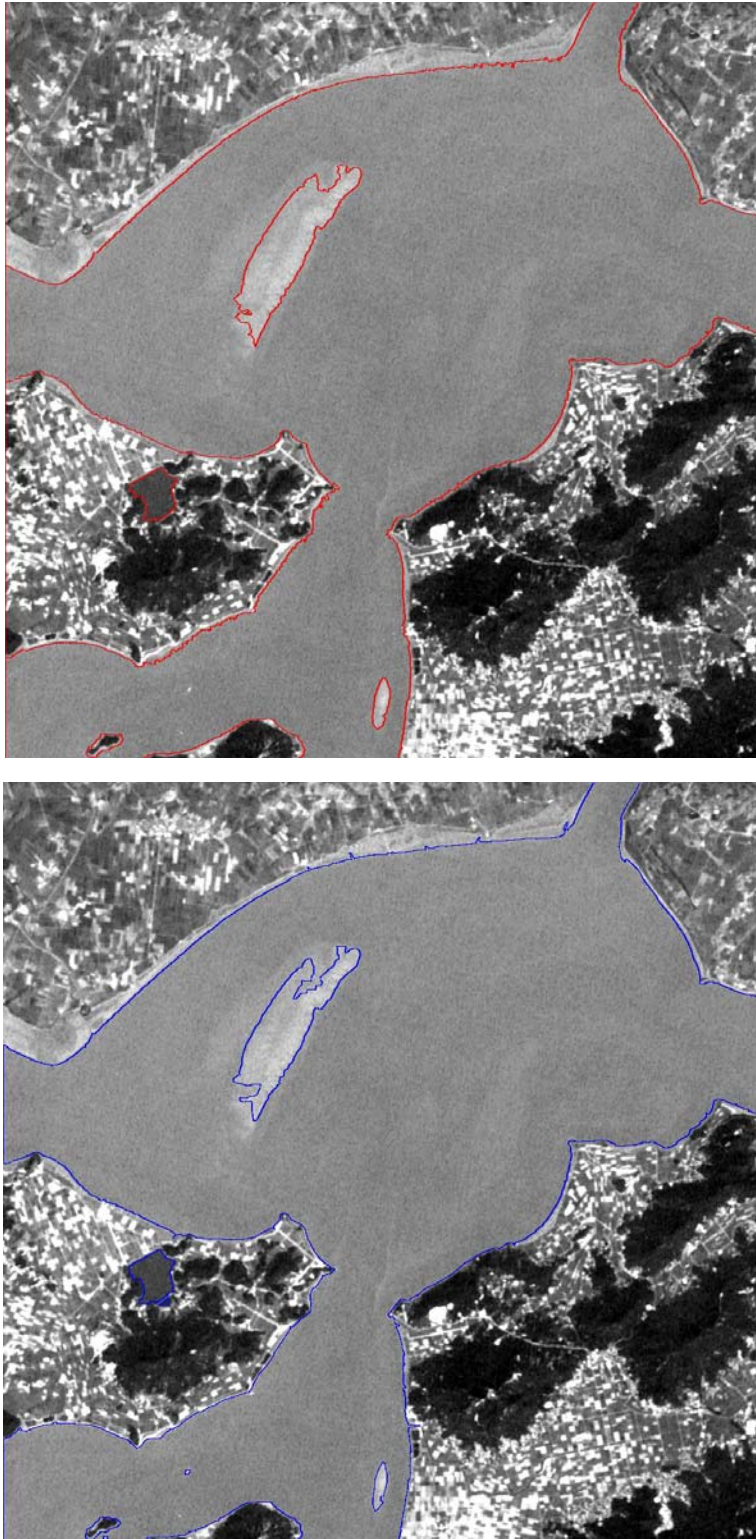
Figure 7-4. Waterline shapefiles. The top panel highlights the original extraction or results file. The bottom panel depicts the waterline after post processing which includes running a Bezier smoothing algorithm to slightly alter the position of vertices.
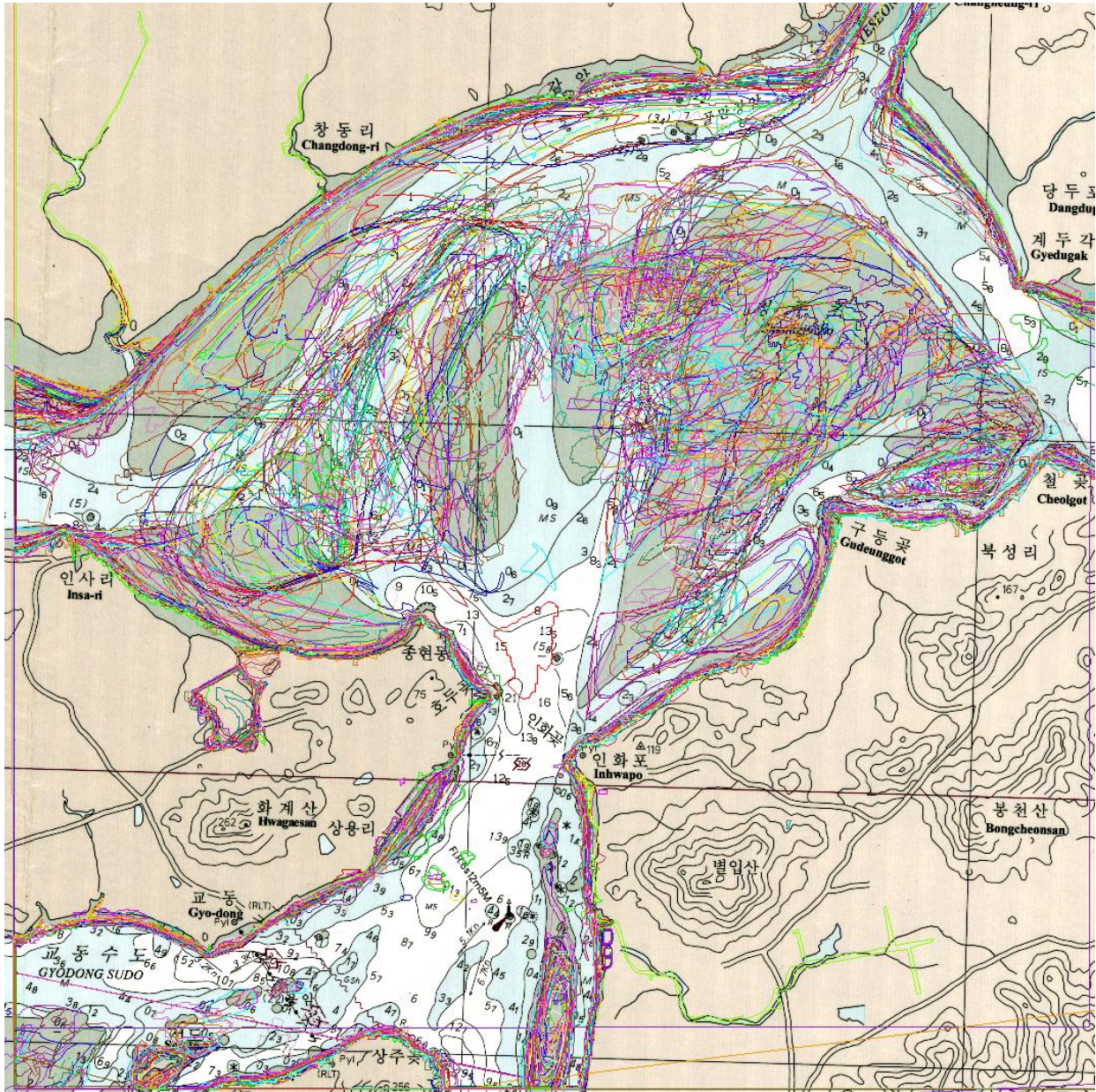
Figure 7-5. 20-year record of waterlines for the HRE. Waterlines include the land-sea boundary for the northeastern tip of Gyodongdo Island and the north western tip of Ganghwa Island. The northern peninsula of Seongomodo Island is located to the south. The Yesung River enters from the north and the Han River enters from the east after passing through the Seoul metropolitan area
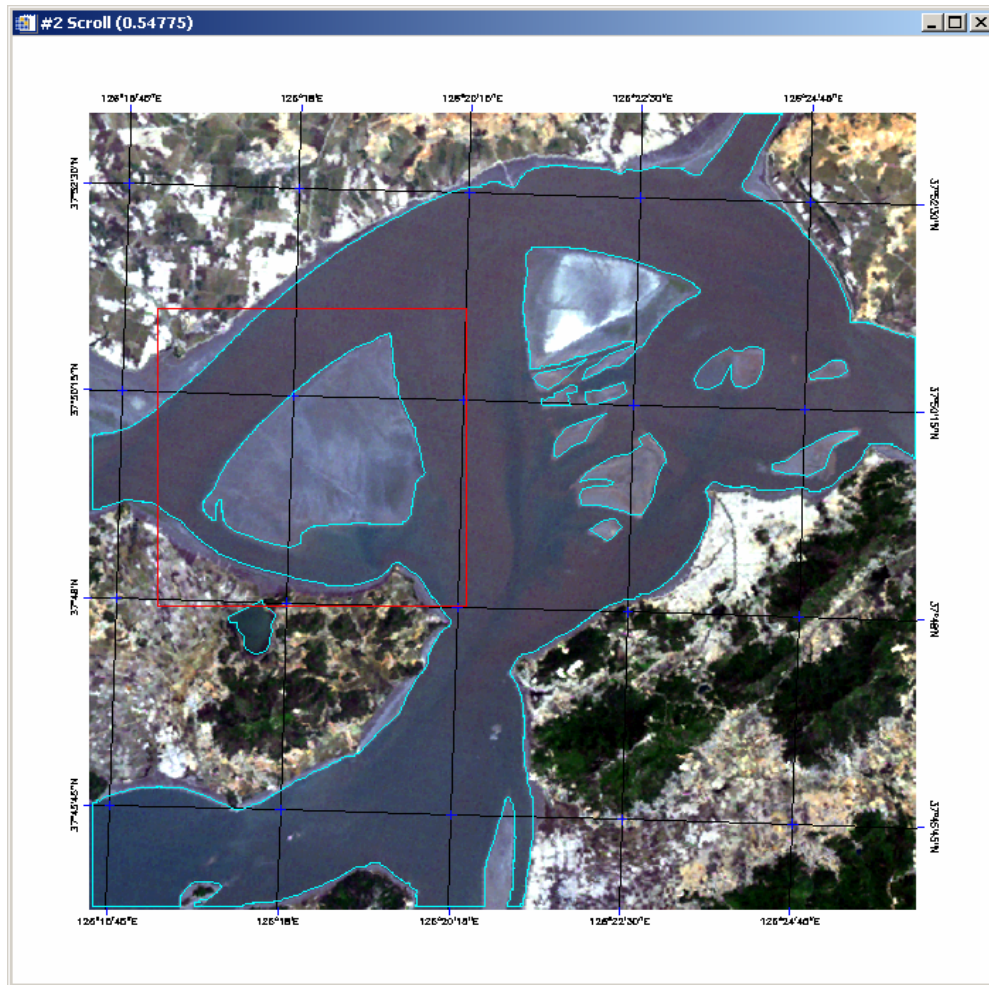
Figure 7-6. Full image (Landsat 4 May 17, 1989) for visual inspection. Black lines are latitude/longitude grid. Blue outlines are waterlines from Feature Analyst® shapefile.

After visual inspection and assessment of the location of edges, feature locations and extent are determined. Most of the noteworthy features are mudflats, though several small islands are visible in some images. Each selected feature is digitized using the ENVI® ROI (Region of Interest) tool (Figure 7-7). ENVI calculates the area of the selected feature, and that value is recorded in the metadata document. The coordinates of the approximate center of the feature are found using the Vector tool and the Cursor Location/Value tool in ENVI®. The Vector tool is used to draw lines to find the center of the particular feature. Then as the cursor is moved over the center, the Cursor Location/Value window will show the latitude and longitude. These coordinates are recorded in the metadata document. As an additional source of feature locations, the user will determine the row(s) and column(s) that the feature spans based on the latitude and longitude grid lines. Those values are also recorded in the metadata.
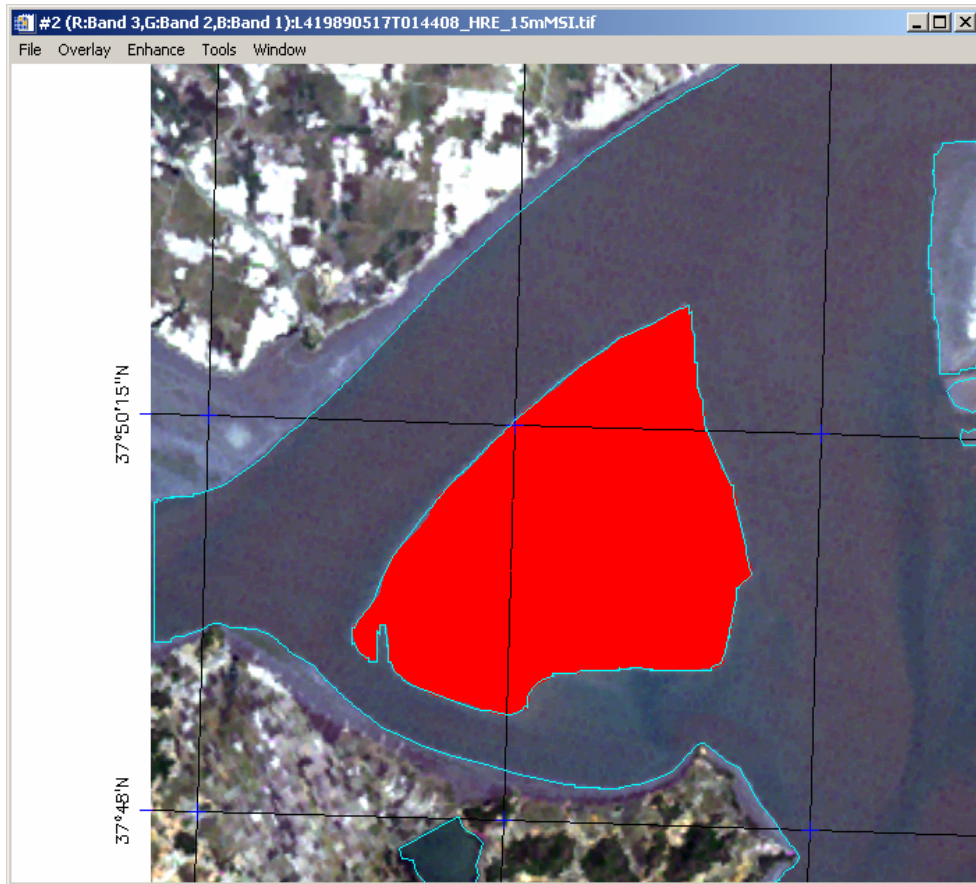
Figure 7-7. ENVI® ROI tool highlighting a large mudflat from Figure 7-6 image. This is a noteworthy mudflat with significant changes in morphology over a 20-year time period.

The metadata document is a text file containing basic information about the image and a table of information about the noteworthy features. Information such as the image date, total number of polygons from the shapefile, and the number of shoals and islands are listed first. Additional information about the image, if any, is included as well. The table lists each shoal, its location in the grid and in latitude and longitude coordinates, its area and a brief description. This description typically explains where the mudflat is in relation to other mudflats or landmasses, and it may include the shape and qualitative size of the feature (i.e., "round, small"). Table 7-3 shows the metadata file corresponding to the image in Figure 7-1. At this point, the latitude, longitude and area values for all polygons are still approximate.

Table 7-3. Metadata for shoals. This shapefile from 17 May 1989 includes 16 polygons highlighting two shorelines and 11 shallow water shoals. Visible shoals are located in the grid locations. The grid is based on lat/lon with spacing set to 2'15" = 5 rows, 6 columns.

Shoal #	Grid Row	Grid Column	Lat	Lon	Area (km^2)	Description
1	2-3	2-3	37.82659	126.30826	10.815	large, N of W landmass
2	2	4-5	37.85546	126.36602	5.67	Large, NE of #1
3	2	4	37.84272	126.35813	0.21825	just S of #2; point on E side
4	2-3	4	37.83854	126.35862	0.16493	just S of #3; curved shape
5	2	4	37.83944	126.36881	0.19238	just E of #4; rectangle shape
6	3	4	37.83227	126.36442	0.29138	S of #4, 5; pointed on E side
7	3	4-5	37.82358	126.37278	1.52	Large, SE of #6
8	3	4	37.81514	126.37001	0.15390	S of #7; pointed on W side
9	2	5	37.84505	126.39605	0.81653	E of #2; curved shape
10	2	6	37.84500	126.41855	0.16988	E of #9; wider on E side
11	3	5-6	37.82897	126.41451	0.57578	S of #10; wider on W side

Notes: There are 2 extremely tiny "shoals" in the southern portion of the image (rows 4-5, columns 3-4) that have not been outlined.

Once the metadata files are complete, the information can be used to determine general statistics about the image region. At this point only the approximate latitudes and longitudes from the Landsat images have been plotted to show a rough time series of mudflat movements over the period between 1989 and 2003. Understanding mudflat changes over time can provide insight into the movements of the surrounding waters. It is also important to note that what looks like one large mudflat in one image can be broken into several smaller mudflats in another image. It would be useful to relate features like this throughout the time series. In future compilations, it would also be useful to include the changes in the area of each shoal as a function of time. Figure 7-8 shows the current version of the mudflat location time series. Note that points may be plotted directly over one another due to the rough location approximation.
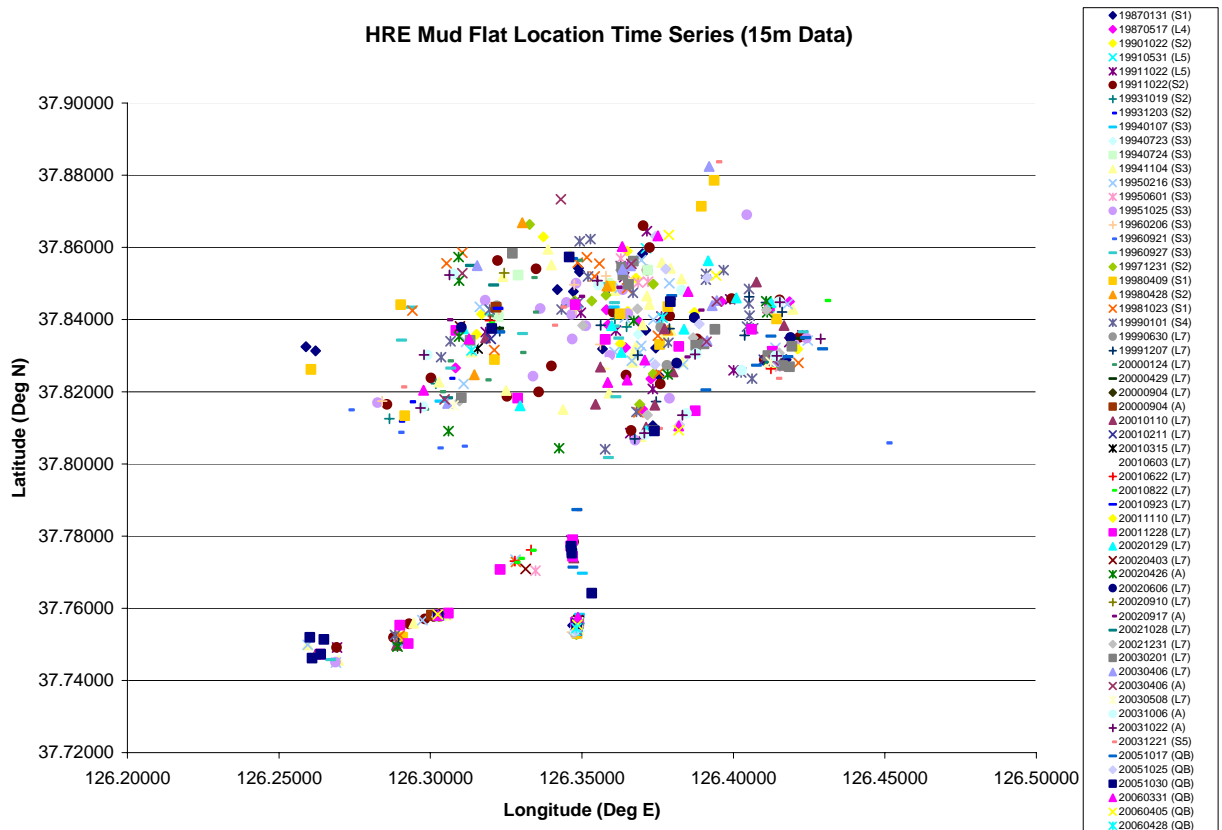
Figure 7-8. Current mudflat location time series. The numbers in the legend indicate the date of the image using the form YYMMDD. Patterns indicate two major mudflats to the north and two more permanent sites to the south.

8. Feature Tracking Analyses and Results

The maximum cross-correlation (MCC) technique is a feature tracking method that may support the identification of flood and ebb channels as well as transport and discharge for selected channels or channel segments.

8.1. Surface Velocities in the Han River Estuary

Imagery analysis, scientific studies, and on-the-scene reports indicate that the HRE presents a complex pattern of circulation. The ebb discharge is approximately 1.78 m^2s^{-1} in the Kyodong waterway which is located east of Kyodong Island (Park et al., 2002). This region borders North and South Korea, a demilitarized zone (DMZ) established during 1953. MCC is especially useful in analyzing circulation patterns since hydrographic surveys in this area are not feasible.

8.1.1. Introduction to MCC and Tracer Equation INVerse

Satellite imaging of littoral regions affords us the opportunity to synoptically image large areas, and offers significant possibilities for characterizing the properties of denied regions. The allure of obtaining river and estuary surface velocities from sequential views of the coastal

domain has been a powerful incentive to spur processing of these image sequences to obtain the velocity maps. This section is concerned with inverting satellite image sequences for surface velocities in the HRE using two techniques and comparing the results. Researchers have used a number of approaches to obtain these vector fields, but two procedures have obtained prominence over the last few decades. The first is the MCC algorithm of Emery et al. (1986), which has been used extensively by oceanographers since then to process satellite data for surface velocities. It has also been utilized to find surface velocities in such diverse applications as ice motion (Ninnis et al. 1986), snow in avalanches (Granada et al. 1995), beach swash zone flows (Holland et al. 2001), atmospheric ozone motion (Gelpke and Kunsch, 2001), and surface velocities on a stream (Bradley et al. 2002).

Another powerful, though less extensively used technique, is the inversion of the heat (or temperature) equation for the velocity vector. For the purposes of this report, we note that the equation is equally applicable for any passive, conserved tracer such as chlorophyll, Color Dissolved Organic Matter, or fine-grained sediment. Two seminal works (Kelly, 1989; Kelly and Strub, 1992) have laid the foundation for this. Using the two-dimensional non-diffusive tracer equation (applied to temperature), they invert sequential AVHRR fields from early NOAA imagers to obtain the surface velocity field and compare the results of their INVerse (INV) technique with surface velocity fields from Acoustic Doppler Current Profilers (ADCP), near-surface drifters, geostrophic velocity profiles from Geosat, and the MCC technique.

The MCC and INV methods have proved to be robust techniques for inversion of image sequences. Each has been used in several different forms and in several locations with satisfactory results. For this report, we apply both techniques to image scenes in the Han River Estuary, but focus on much finer temporal and spatial resolution scales than any of those employed in the above papers. We do this by using imagery from commercial high-resolution satellites. We also compare results from the two image processing methods, discuss the viability of using either technique in the region, and suggest improvements to make the technique more versatile.

8.1.2. Multi-source Imagery of HRE

Velocity retrievals have typically been performed in the open ocean using AVHRR imagery with a resolution of 1.47 kilometers. However, rivers and estuaries having widths the order of a few kilometers require imagery with far smaller pixels. For this purpose, we have found it useful to employ the visible channels in both Landsat ETM+ and ASTER images. These have resolutions of 30 m and 15 m respectively, and can better resolve surface expressions of the finer scale bathymetry- and shore-induced phenomena present in tidal estuarine and riverine flows. A drawback in tracking visible features has to do with the nature and sources of the biological or sedimentary material responsible for the contrast in the image. Tracer features arise when biota and sediments from the coastline or bottom are introduced, and contrast with the ambient fluid. Such contrasts are also introduced at river confluences. Once introduced, their evolution is that of a long-lived streak line as it is deformed by the flow.

This study uses nearly contemporaneous spaceborne imagery from Landsat-7 and ASTER. Both sensors have similar wavelength ranges in the following visible and near-infrared:

Landsat bands (2, 3, 4) = (565, 660, and 825 nm) and ASTER bands (1, 2, 3) = (556, 661, and 807 nm). Since the full width of half magnitude (FWHM) is 60-150 nm for Landsat and 60-100 nm for ASTER, the differences in center wavelengths are smaller than the spread of each band. The Landsat and ASTER bands are effectively identical. Consequently, images synthesized from these bands show features with essentially the same spectral signature, and may be used for feature tracking to derive surface velocity distributions from pairs of scenes that were imaged at almost the same time.

We have obtained two pairs of Landsat / ASTER images on two separate days, September 4, 2000 and April 6, 2003. Table 8-1 provides details about these images. To represent the flow optimally, we exhibit the bands having the best contrast; these are also listed in Table 8-1.

Table 8-1. Sensor, dates, times, and bands used for velocity calculations.

Sensor	Date	Time (UT)	Band Used
Landsat 7	September 4, 2000	02:01	3
ASTER	September 4, 2000	02:43	2
Landsat 7	April 6, 2003	01:59	4
ASTER	April 6, 2003	02:29	3

On September 4, 2000, the images are separated by 42 min (Table 8-1), and we can obtain a sense of the motion by comparing the two images. In Figure 8-1, we show the Landsat and ASTER images, and three hydrodynamic features are evident.

September 4, 2000

02:01 UT   02:43 UT

Landsat 7 (Band 3)   ASTER (Band 2)

Figure 8-1. Landsat (left panel) and ASTER (right panel) images on September 4, 2000. The time separation is 42 min.

First, it is clear that the water is moving generally from the northern inlet, across the basin, and out the southern tributary. This constitutes a north-south axis of the flow across the estuary. Second, no obvious flow pattern exists to either side of this axis; motion is obviously present and we conjecture that large scale turbulent eddies may dominate the flow there. And third, the currents are likely quite large, as much of the tracer exhibits significant kinematic distortion. That is, few identifiable advected "blobs" exist; instead, the tracer appears to have been strained out into long filaments.

Table 8-1 reveals that on April 6, 2003, the two images are separated by only 30 min. Comparison of the two scenes in Figure 8-2 shows that the sense of the flow is opposite from that in Figure 8-1. There is a clear indication that the dominant flow along the estuarine axis is from the southern tributary, across the estuary, and out the northern channel. In addition, the sandbar between the northern and western tributaries is exposed, and appears to approximately double its area in the thirty-minute interval.

April 6, 2003

01:59 UT
Landsat 7 (Band 4)

02:29 UT
ASTER (Band 3)
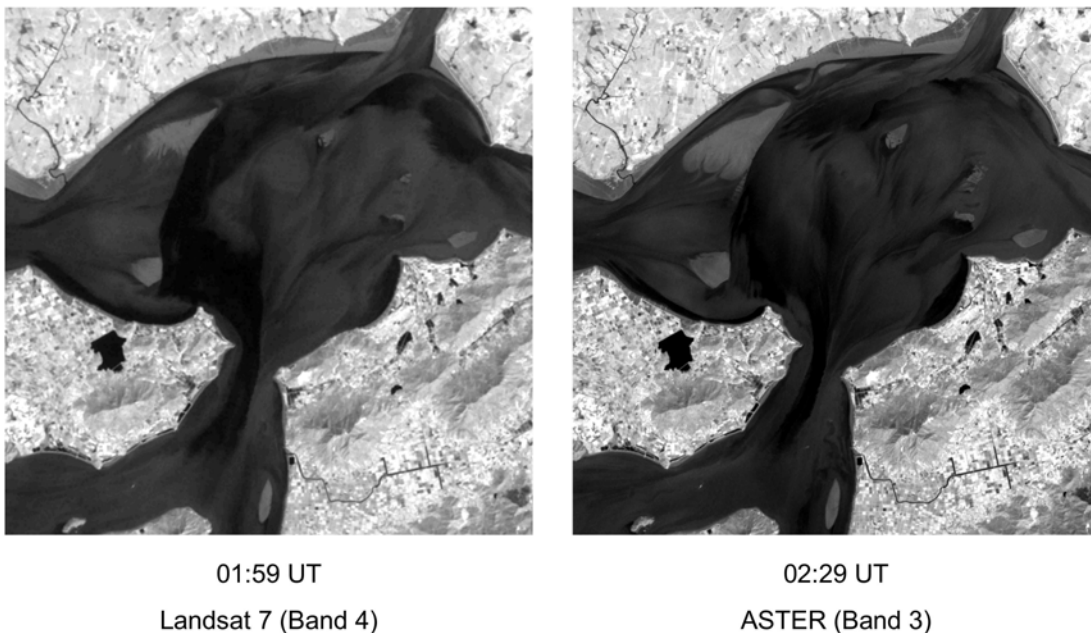
Figure 8-2. Landsat (left panel) and ASTER (right panel) images on April 6, 2003. The time separation is 30 min.

8.1.3 Calculated Surface Velocities

The image pairs in Figures 8-1 and 8-2 contain information on the advection and straining of the surface tracer, which may be processed to obtain a surface velocity field over the estuary. To do this, we employ two different techniques, the MCC and the Tracer equation INVerse (INV). Emery et al. (1986) document the MCC, while Kelly and Strub (1992) give details about the INV method. Because of the ample literature that exists on both methods, it seems

35

superfluous to discuss either one at length here. Nevertheless, a brief mention of how we employ each is appropriate. A synopsis and comparison of each appears in Figure 8-3.

Velocity from Image Sequences
Established Techniques

Maximum Cross Correlation

$t = t_0$ $t = t_1$

- Pass t_1 image over t_0 image
- Perform cross correlation:

$$C(\Delta \vec{x}) = \langle T(\vec{x}, t_0), T(\vec{x} + \Delta \vec{x}, t_1) \rangle$$

- Max correlation $\longrightarrow \Delta \vec{x}_{max}$
- Define $\vec{u} = \Delta \vec{x}_{max} / \Delta t$
- Move 1 pixel & repeat $\longrightarrow \vec{u}_{ij}$ field

Tracer Equation $\left(\partial T / \partial t + \vec{u} \cdot \nabla T = 0 \right)$

- Inversion based on 9-pixel sub-images
- Images yield $T, \partial T / \partial t$ & ∇T at each point
- Assume $\vec{u}$ constant over 9 points
- Invert 9 equations for $\vec{u} = (u, v)$ pairs

  -- Over-determined system

  -- Least squares solution

- Move 1 pixel & repeat $\longrightarrow \vec{u}_{ij}$ field

**Figure 8-3. Synopsis of the MCC and Tracer Equation Inversion techniques to obtain velocities.**

The MCC starts with the first image (at time t_0), and correlates it with the second image (at time t_1), which is displaced a vector distance $\Delta \vec{x}$. The displacement that produces the largest value of the cross correlation between the two images is the velocity $\Delta \vec{x}_{max} / \Delta t$ for the local point in the t_0 image from which the displacements $\Delta \vec{x}$ are measured (see left column of Figure 8-3).

The INV assumes that the eight pixels, which surround the point of interest, have the same velocity, but that the variables T, ∇T, and $\partial T / \partial t$ are either known or may be calculated at each of the surrounding eight points from the values in the image. Cast in this way, the horizontal divergence is not constrained to vanish, and the inversion is an over-determined system, which may be solved for the velocity (see right column of Figure 8-3).

We show the results of these velocity estimates for 4 September 2000 (see Figure 8-1) in Figure 8-4. The velocities derived with the MCC are shown in Figure 8-4 panels (a) while those from the INV appear in panel (b). Velocity results for 6 April 2003 are similarly shown in Figure 8-5 (a) and (b) for the two techniques.
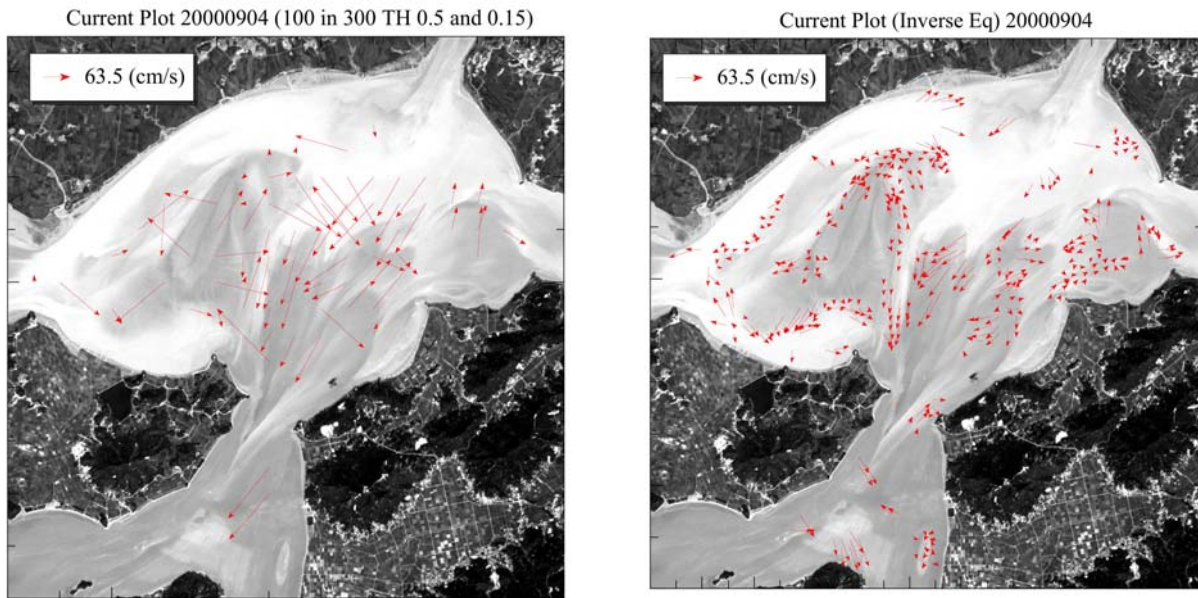
Figure 8-4. Feature tracking techniques for September 4, 2000. Panel (a) depicts velocity fields for September 4, 2000 obtained using MCC technique. Panel (b) depicts velocity fields for September 4, 2000 obtained using the INV technique.
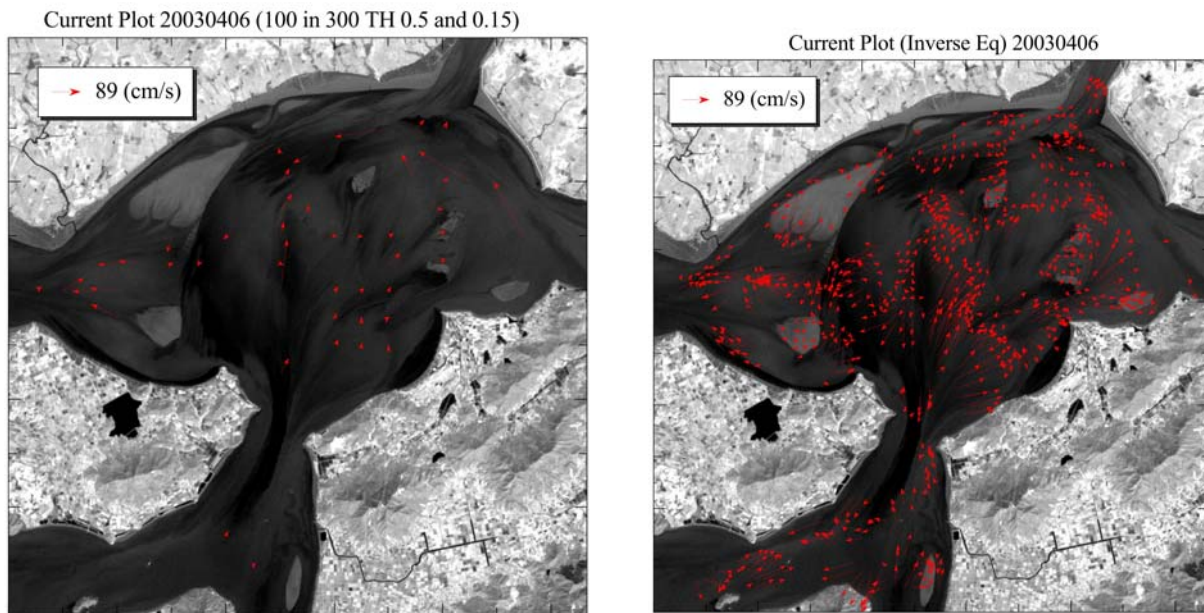
Figure 8-5. Feature tracking techniques for April 6, 2003. Panel (a) depicts velocity fields for April 6, 2003 obtained using the MCC technique. Panel (b) depicts velocity fields for April 6, 2003 obtained with the INV technique.

8.2 Quality Assurance of Feature Tracking Methods

An issue with all remote determinations of surface velocity is the accuracy of the result. Without *in situ* observations, validation of the results is all but impossible. Something that can be accomplished, however, is to impose a self-consistency test upon the results. In ocean regions, velocities derived from AVHRR imagery, for example, can be subjected to a nearest-neighbor self-consistency test to determine their mutual compatibility. For many estuary applications, spatial variability of the flow over short distances makes this difficult. To remedy this deficit, we examine instead the histogram of the correlation values. Such a histogram distribution of the correlation values appears in Figure 8-6 (a) and is an example of an MCC calculation yielding credible results. Note in particular that as the value of the contour is increased (i.e., larger correlation coefficients), there are fewer pixels with that value. In other words, the histogram is monotonic-decreasing for the larger values of the correlation coefficient. Therefore, we have confidence in this result, as the local maximum value is well resolved and unique.

The situation portrayed in Figure 8-6 (a) yields valid points, but qualitatively different behavior can be demonstrated as well. In Figure 8-6 panel (b) we display a correlation/histogram pair with a large plateau-like region surrounding the local maximum. The correlation contours in Figure 8-6 (b) appear at least superficially acceptable, but closer examination reveals that the contour with the largest correlation coefficient is a meandering line that encircles a relatively large region. Locating a meaningful maximum value is effectively impossible, because of the ambiguity in its location. The histogram of the contour population conveys the same fact: As the contour level is increased, the number of contours with that value increases as well. Together, the correlation contours and their population histogram indicate that the resulting velocity estimate is likely to be unreliable. This may not be surprising, as some of the regions of the source image are featureless. Moreover, we have found that the strategy of utilizing MCC with the gradients of the images is not effective here. This occurs because the gradient operator tends to level, or smooth, the pixel-to-pixel tracer variation across the image. However, it is noteworthy that the essential diagnostic technique described here is effective with not only the MCC, but the INV velocities as well.

8.3. Feature Tracking Application for HALE

Comparison of the results from both inversion techniques is useful for three reasons. First, it is imperative to know if they agree and to what extent. Second, examination of the results is crucial to determining which technique is more appropriate for measuring the flow. Third, it may be possible to see how to improve the application of the technique.

The results in Figure 8-4 reveal a picture of a somewhat confused flow. The vector arrows in 8-4 (a) display MCC vectors that have no clear general sense of direction. It is generally true that many vectors along the north-south central estuary axis indicate a tendency for a southward-directed flow, but many arrows are also directed across-stream. Much of this conflicting behavior results from the nature of the MCC method. The correlation box sizes for this velocity map are necessarily large (a 100 X 100 pixel square inside a 300 X 300 square), because the large velocities present mandate a commensurately large box to capture the motion. In essence, the

window must be sufficiently large that a feature is not advected out of it within the time interval
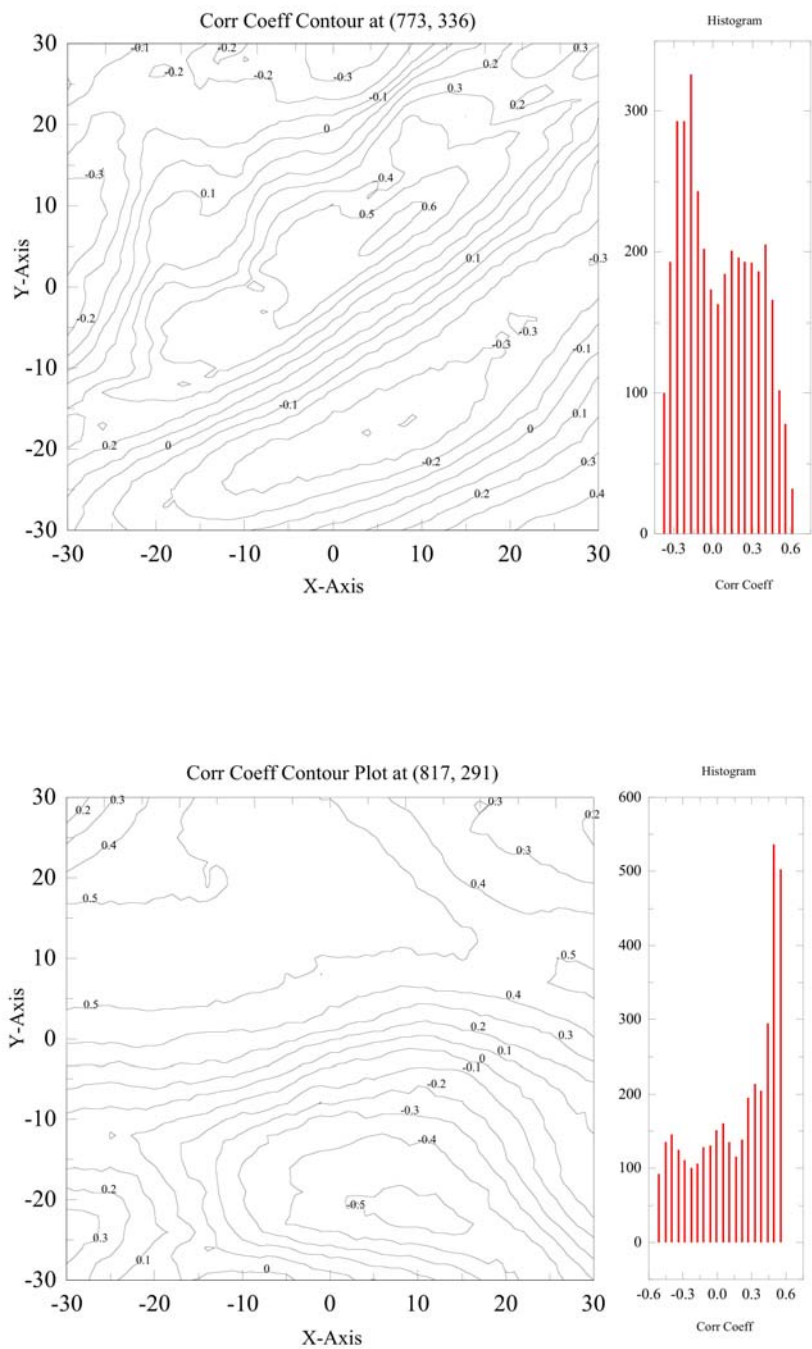
Figure 8-6. Quality Assurance measures for feature tracking. The top panel (a) depicts a well-defined local correlation coefficient maximum and the associated histogram for the surrounding points is shown. The bottom panel (b) shows a poorly defined local correlation coefficient maximum and the associated histogram for the surrounding points are shown.

between the images. The overall size of the image is 1067 X 1067 pixels, and the areas of suspected sandbars must be masked off, so that the correlation calculation is not contaminated with stationary parts of the image. These two considerations of size and geometry limit our flexibility to determine an accurate, basin-wide velocity map.

In contrast to the restrictions inherent in the MCC, the INV exhibits much better resolution. From Figure 8-3, we see the reason is that the technique uses only a 3 X 3 pixel square, which is more suited to capturing the small-scale detail present around the sand bars, as well as that in the turbulent flow. It is clear from Figure 8-4 (b) that there is a great deal of detail present within the flow that is not apparent in the MCC calculation. For example, it is now clear that there is a strong flow from north to south, and that water is diverted around the sandbar to the west of estuary center. Several additional flow features are present, and the chaotic nature of the flow to either side of the north-south axis is evident. Additional analyses may even be able to estimate times to flood or expose mudflats.

Apart from the issue of the different levels of detail available in the MCC and INV velocity maps, the two methods differ significantly in the magnitudes of the velocities represented (Figure 8-4 a and b) by a factor of two, and this is presently not understood. The sparseness of detail present in the MCC (Figure 8-4 a) and the conflicting vector directions lead us to suspect that the MCC results may not be trustworthy, and the large time interval (42 min) between images may be the cause.

In contrast with this long time interval, the images from 6 April 2003 show a somewhat more compatible picture between the MCC (Figure 8-5 a) and INV (Figure 8-5 b) results. In particular, there is a south-to-north flow evident across the estuary, and both velocity maps capture the efflux out the west tributary. Moreover, the velocity magnitudes are in rough agreement, with maximum magnitudes being of the order of 90 cm/sec in each technique. Furthermore, the detail of the flow off the sandbar in the west as it is exposed between the two images is evident in small velocities directed outward. While it is true that both techniques yield comparable velocities for this image pair, the resolution of detail available with the INV technique makes this algorithm the preferred one. Given the appropriate pairs of images this technique could be applied to investigate the exchange of water between the HRE and Kyunggi Bay.

8.4. Summary of Feature Tracking Applications

In this section, we have worked with commercial satellite images having a pixel size of 15 m (ASTER) and 30 m (Landsat 7) on two days, September 4, 2000 and April 6, 2003. We have used the displayed velocity maps from the two days using the MCC and INV methods. Although our data set is comprised of only four images, several conclusions emerge and are self-consistent. They are as follows:

- The MCC technique is too coarse, and the Han River flow is too rapid for the method to give useful results with the time separation we have available between the satellites. Results from the images separated by 42 min. are very suspect, while the 30 min

separation produces somewhat more believable results.

- The INV technique, by its limited demands on size of the required pixel square, yields a much denser set of velocity vectors. In addition, small-scale details of the flow are captured, such as the flow around the sandbars and the converging flows entering the tributaries.
- The flow in the second set of images (April 6, 2003---Figure 8-5) has more features amenable to tracking in the near infrared bands around 800 nm than the Figure 8-4 image. This may be due to the fact that the velocity is larger (89 cm/sec vs. 62.5 cm/sec) and the levels of near-bottom turbulence are greater in Figure 8-5. This turbulence leads to more suspended sediment from the bottom boundary layer, which is more readily imaged in the longer wavelength bands.

Our principal conclusion is that the Tracer equation inverse technique is a viable method for use in the HRE, provided the time interval is reduced to be compatible with the rapid tidal flow. An estimate of the required maximum separation can be obtained by using a Courant, Friedricks, Levy (CFL) estimate for the current calculation. If the advection speed is designated by c, the time between images by Δt, and the size of the 3 X 3 calculation window for the inverse technique as Δx, the time interval is constrained to be

$$\Delta t \leq \Delta x/c.$$

From Fig 8-5 (b), c ~ 0.9 m/s, and we have used a computational window of $\Delta x = 1000$ m. Consequently, we required $\Delta t \leq 1100$ s. This is less than the actual separation time (30 min, or 1800 s) between the images used to create the velocity field in Figure 8-5 (b). Obviously, the images are too far separated in time to give a result rigorously consistent with a CFL criterion. At the same time, there is too much spatial variability in the estuary to merit increasing the computational window (Δx) beyond its current value of 1 km. Clearly, smaller separation times between the images would yield more accurate estimates, and this refinement must be pursued.

9. High-Precision Digital Elevation Model

High resolution elevation data for the HRE region was produced by Marine Corps Intelligence Activity during February 2006 as a 1º by 1º matrix of elevation data in a signed 16-bit GeoTIFF format. The vertical reference is Mean High Water. Horizontal spacing is 10m by 10m. Vertical units are in whole meters.

In building the DEM, stereo imagery is auto-correlated in Socet Set® to create an initial digital terrain model (DTM) and then manually edited by trained stereo technicians so elevation posts fall within assigned tolerances and model bare earth elevations. Water (open water, rivers, lakes, etc.), built-up areas, and heavily vegetated areas are specifically addressed using an advanced suite of area-processing tools. Also, a number of geomorphic tools are used to fine-tune linear features, such as single line drains, ridge lines, etc. The data is reviewed throughout the process and quality control checkpoints are injected to ensure the data is horizontally and vertically accurate. Marine Corps Intelligence Activity extracted their shorelines at the high water/debris line with open water elevation set to zero. 90% of elevation posts are edited within 3 meters of bald-earth as seen on imagery. A DEM with an extracted waterline from a QuickBird™ image is provided in Figure 9-1. There are several candidate positions to extend a

beach profile perpendicular to the shore to build a depth profile. The profile will be done during Phase II.
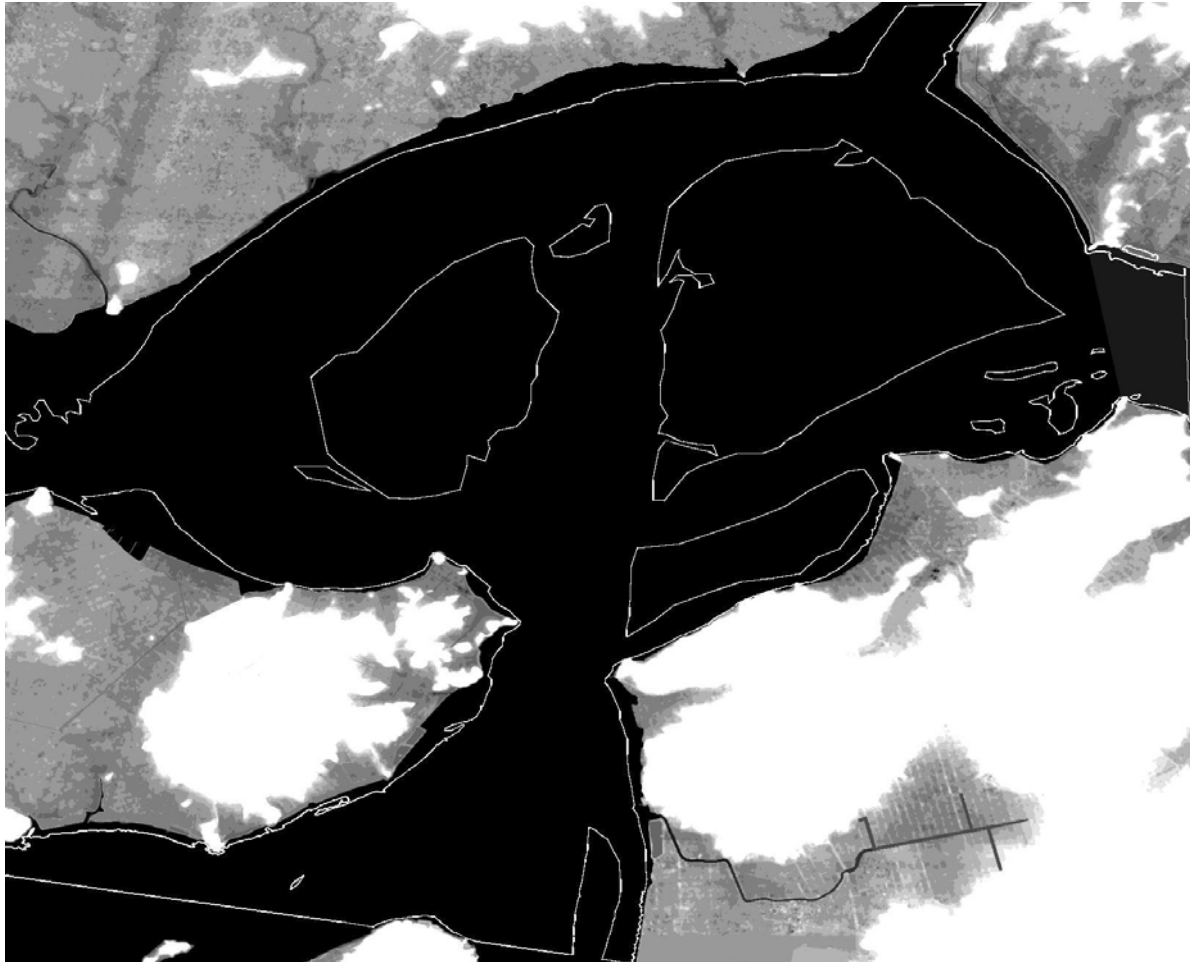
Figure 9-1. Waterline overlayed on a high-precision DEM. Once reference locations are determined, and shore normal transects drawn, a profile will be extended that intersects with the 66 waterlines. Depths will be pulled off of the waterlines and times noted from the waterline file.

10. Tidal Curves from Remote Sensing Imagery

The preferred observational data for predicting tides is a continuous curve from an automated water level gauge, sampled at hourly (or shorter) intervals. In denied regions, however, data of this sort is virtually impossible to obtain, so we remedy the deficit with data from remote images. A synthetic time series has been generated for a customized harmonic analysis application to plot a tidal time series from imagery-derived shoreline fluctuations (See Appendix D).

Using remote sensing image sequences poses two challenges. First, the waterline locations must be converted to a time series of water height. A DEM is used to estimate these depths, based on waterlines that are extracted from the image time series. The resultant curve will be used to predict tides, but our experience indicates there is insufficient data to obtain more than 3-

4 tide height realizations per year on average, which poses the second challenge: how do we use a severely under-sampled time series to obtain amplitudes of tidal constituents with periods of as little as 12 hr?

The strategy we employ involves fitting the image-derived elevations to a harmonic curve at discrete points in time (t_i) that are representative of the tidal elevation:

$$\zeta(t_i) = \sum_{n=0}^{N} \left[a_n \cos \omega_n (t_i - t_0) + b_n \sin \omega_n (t_i - t_0) \right],$$ (1)

where

$a_0 =$ computed mean water level,
$a_n, b_n =$ derived amplitudes,
$N = 7$ (four major semidiurnal and three diurnal constituent periods),
$t_i =$ image time, and
$t_0 =$ midpoint of 20-year imagery time series
$\omega_n =$ frequency of each tidal constituent, with $\omega_0 \equiv 0$.

The phases of the constituents of the actual tide may not necessarily coincide with the phases of the equilibrium tide, i.e., the tidal elevation in the open ocean nearest the location of interest in the Han River. Instead, differences in phase propagation speeds of the individual constituents, the retarding effect of bottom friction, and river morphology introduce changes to the elevation forced at the river mouth. Moreover, these processes are continuously at work as the tide propagates up-river, so that the coefficients in equation (1) vary by locality. For this reason, we allow for the possibility of the phase shift of one constituent with respect to any other, and use both sines and cosines. For a given location, amplitudes and phase lags together are called harmonic constants.

If we define the quantities

$$\zeta_i \equiv \zeta(t_i),$$
$$A_{in} \equiv \cos \omega_n (t_i - t_0), \text{ and}$$
$$B_{in} \equiv \sin \omega_n (t_i - t_0),$$

we may write (1) as

$$\zeta_i = \sum_{n=0}^{7} \left(a_n A_{in} + b_n B_{in} \right).$$ (2)

We may obtain the 16 coefficients ($a_n, \text{ and } b_n$) by least squares fitting equation (2) to the 66 image-derived ζ_i, which is tantamount to minimizing the following expression.

$$e = \sum_{i=1}^{I} \left[\sum_{n=0}^{N} \left(a_n A_{in} + b_n B_{in} - \zeta_i \right)^2 \right].$$

43

The requirements that $\partial e/\partial a_j$ and $\partial e/\partial b_j$ vanish lead to

$$\sum_{n=0}^{N}\sum_{i=1}^{I}\left(a_n\,A_{in}\,A_{ij} + b_n\,B_{in}A_{ij}\right) = \sum_{i=1}^{I}\zeta_i\,A_{ij}$$

$$\sum_{n=0}^{N}\sum_{i=1}^{I}\left(a_n\,A_{in}\,B_{ij} + b_n\,B_{in}B_{ij}\right) = \sum_{i=1}^{I}\zeta_i\,B_{ij}$$

(3)

for $1 \le j \le 8$. Here, we have interchanged the order of the sums over i and n, and used the identity $\partial\left(a_n\,A_{in}\right)/\partial a_j = A_{in}\,\partial a_n/\partial a_j = A_{in}\,\delta_{nj} = A_{ij}$ and similarly for the b_n. The equations (3) constitute $2\,(N+1)$ equations for the unknowns, and I $= 66$. This $2\,(N+1)\,X\,2\,(N+1)$ set may be solved using a number of IDL routines.

This is not a standard approach, but it is mandated by the sparseness of the data. Traditional harmonic analysis techniques rely on long time series of continuous measurements that are separated into a number of harmonic constituents. The quantities that are derived are harmonic constants that consist of amplitudes and phase relationships. For the present work, we supply the frequencies of the individual constituents, with the assumption that the frequency is unchanged by the propagation within the river.

The time required for a constituent to pass through a complete cycle is known as its period and is determined by dividing 360º by the speed (º/hr). Speeds are derived from astronomical data. The seven major constituent periods are provided in Table 10-1.

Table 10-1. Constituent periods in hours. These periods are derived from astronomical data and are independent of the locality.

Name	Code	Period ($= 2\pi/\omega_i$)
Principal Lunar	M_2	12.420601220441357204339611779934
Principal Solar	S_2	12.000000000000000000000000000000
Larger Lunar Elliptic	N_2	12.658348200328880764042144760758
Luni-Solar Semidiurnal	K_2	11.967234827982900097935860753936
Luni-Solar Diurnal	K_1	23.934469655965800185871721507872
Principal Lunar Diurnal	O_1	25.819341664737627149141037838274
Principal Solar Diurnal	P_1	24.065885978238823702277180980944

It is crucial that we know the periods very accurately, since our image record extends over 19 years. We nominally require that we be able to place the zero crossing of a sinusoidal oscillation to within, say, 10 min. after 9.5 years, since we are choosing t_0 as the mid point of the tidal record. With this criterion, we may calculate the accuracy required.

Suppose we have two estimates of the M_2 period; call them $\omega^{(1)}$ and $\omega^{(2)}$. Each sine wave will have a zero crossing at times $t^{(1)}$ and $t^{(2)}$, respectively, provided

$$\omega^{(1)}\,t^{(1)} = 2\pi n = \omega^{(2)}\,t^{(2)},$$

44

where n represents many years of tidal cycles. Clearly, ωt = constant, so that

$$\frac{d\omega}{\omega} = -\frac{dt}{t}.$$

If we specify an accuracy (zero crossing) to within $dt = 10$ min, $t = 9.5$ yr X 365 days X 24 hr X 60 min, then $d\omega/\omega \sim 2 \cdot 10^{-6}$. Since an accuracy in frequency of two parts in a million is required to specify the placement of the zero crossing of the M_2 tide to within ten minutes, the 30-place accuracies in Table 1 suffice by a wide margin.

11. Conclusions and Recommendations

The determination of coastal tidal elevations remains a difficult problem without the measurement of water level elevations by a tide gauge. Phase I has demonstrated that we can build an imagery stack from commercial imagery that provides approximately three to four images per year on average. From these images we can extract waterlines that provide the basis to build a time series of water level fluctuations from a reference profile. Other imagery analysis procedures such as feature tracking can be used to assess complex circulation patterns. Some hydrodynamic agents such as high turbidity may confound selection of waterlines. These imagery-derived water levels will be compared with the synthetic time series that has been generated for Phase II of this project that was introduced in Section 10. The differences include errors that occurred between both imagery analysis and tidal predictions. The harmonic predictions only include astronomical forces. Water levels are impacted by river flow and winds.

As soon as the correct DEM is obtained, a time series of tidal height versus time will be obtained. Extraction of tidal constituents from inconsistent data is a research project that involves determining required number of data points to authoritatively repeat a harmonic curve that is the superposition of seven components. Our sparse dataset renders the application of wavelets as inappropriate. Harmonic analysis and Singular Spectrum Analysis (SSA) are techniques that are being experimented with during Phase II. This work is using a synthetic series obtained from the predictions at Total Tide Station 7480 located at Oep'ori at 37º 42' N; 126º 22' E for each of the 66 image files. A synthetic data set from a NOAA tide gauge must be built to experiment with signal processing.

A geodatabase should be developed so that other hydrodynamic agents can be analyzed and saved in a GIS environment. The waterlines can be viewed as contours of the intertidal and could be combined into representative bands based on other tidal datums. They allow a planner to evaluate how much beach is available at the time of imaging, over selected months, seasons, significant meteorological events, etc. They might be used to build mudflat DEMs that are based on season. The waterlines can be used to determine wetted perimeter and with other algorithms such as INV might compute transport or with Manning's equation estimate depths.

12. Acknowledgments

Geospatial-Intelligence Agency's InnoVision Directorate and the Naval Research Laboratory's Remote Sensing Division. This project benefits from early efforts by LCMD Douglas Lamb, who researched background information and collected commercial satellite images. Efforts by Messrs. Tim Craig and John Bradley were also instrumental in obtaining necessary data and information from NGA. Special thanks to Dr. David A. Jay from University of Portland for his seminar, suggestions and comments.

13. References

Bird, E.C.F., and M.L. Schwartz, 1985. *The World's Coastline*, New York, N.Y.: Von Nostrand Reinhold Company, Inc., 1071 pp.

Boicourt, W.C. 1993. Estuaries: Where the river meets the sea. *Oceanus* 36(2): 29-37.

Bradley, A.A., A. Kruger, E.A. Meselhe, and M.V.I. Muste (2002) Flow measurement in streams using video imagery, *Wat. Resourc. Res.38*, 1315-1326.

Choi, K.S., R.W. Dalrymple, S.S. Chun, and S.-P. Kim, 2004. Sedimontology of Modern, Inclined Heterolithic Stratification (IHS) in the Macrotidal Han River delta, Korea. Journal of Sedimentary Research, 74(5): 677 - 689.

Climate Analysis Branch, NOAA, International Comprehensive Ocean-Atmosphere Data Set (ICOADS), Available online. URL: http://icoads.noaa.gov. Accessed on January 16, 2007.

Dean, R.G. 1991. "Equilibrium Beach Profiles: Principles and Applications." *Journal of Coastal Research*. Volume 7, Number 1. Pages 53 to 84.

Emery, W.J., A.C. Thomas, M.J. Collins, W.R. Crawford, and D.L. Mackas (1986), An objective method for computing advective surface velocities from sequential infrared satellite images, *J. Geophys. Res.,91,* 12865-12878.

Granada, F., O. Marco, and P. Villemain (1995), Use of imaging techniques for velocity mapping on the surface of a dense avalanche, *Houille Blanche-Revue Internationale de Eau, 50,* 69-75.

Gelpke, V. and H.R. Kunsch (2001), Estimation of motion from sequences of images: Daily variability of Total Ozone Mapping Spectrometer ozone data, *J. Geophys. Res., 106,* 11825-11834.

Golyandina, N., V. Nekrutkin, and A. Zhigljavsky, *Analysis of Time Series Structure: SSA and related Techniques*, London, United Kingdom: Chapman & Hall/CRC, 2001

Guide to Coastal North Carolina: Barrier Island Dynamics, Available Online, http://ncnatural.com/Coast/dynamics.html, Accessed on July 21, 2006

Hicks, S.D., 2000. Tide and Current Glossary, National Ocean Service, National Oceanic and

Atmospheric Administration, Silver Spring, MD, 29 pp.

Holland, K.T., J.A. Puleo, and T.N. Kooney (2001), Quantification of swash flows using vide-based particle image velocimetry, *Coast. Eng. 44,* 65-77.

Jay, D. A. and T. Kukulka, 2003, Revising the paradigm of tidal analysis--the uses of non-stationary data, Ocean Dynamics 53: 110-125.

Kelly, K.A., "An Inverse Model for Near-Surface Velocity from Infrared Images," *J. Phys. Ocean.*, vol. 19, pp. 1845-1864 (1989).

Kelly, K.A., "Correction", *J. Geophys. Res.*, vol. 97, 12767-12767 (1994).

Kelly, K.A. and P.T. Strub, (1992) "Comparison of Velocity Estimates from Advanced Very High-Resolution Radiometer in the Coastal Transition Zone," *J. Geophys. Res. Res.*, vol. 97, pp. 9653-9668.

Marine Corps Intelligence Activity. *Generic Information Requirements Handbook.* MCIA-1540-002-95, Quantico, VA: United States Marine Corps, 1995.

McDermid, J.G., M.D. Earle, D.C. Herringshaw, S.M. Mayfield, C.R. Nichols, 1997. METOC Conditions Affecting AAAV Ship-to-Objective Maneuver: A Detailed Analysis of Power Projection Points Sited on the Iranian and Korean Coasts, NRL Memorandum Report. NRL/MR/7170—97-8060, Naval Research Laboratory, Stennis Space Center, MS.

MCIA, Republic of Korea Country Handbook. DoD-2630-KS-002-00, Quantico, VA: United States Marine Corps Intelligence Activity, 2000

Naval Research Laboratory, 1995. North and South Korean regional Conflict Environmental Assessment Guide for Selected Areas, NRL/AE/717X—9X-000X, Naval Research Laboratory. Stennis Space Center, MS.

Nichols, C.R., D. Lamb, T. Donato, and X. -H. Yan, 2004. Oceanographic Information Collection and Data Availability for the Han River Estuary, NRL Memorandum Report, NRL/MR/7205—04-8837, Naval Research Laboratory, Washington, D.C.

Ninnis, R.M., W.J. Emery, and M.J. Collins (1986), Automated extraction of pack ice motion from Advanced Very High Resolution Radiometer Imagery, *J. Geophys. Res, 91,* 10725-10734.

Park, K. J.-H. Oh, H.-S. Kim, and H.-H. Im, 2002. Case Study, Mass Transport Mechanism in Kyunggi Bay around Han River Mouth, Korea. J. of Hydraulic Engineering, 128 (3), 257-267

Parker, B. B., 1991. Tidal Hydrodynamics. New York, NY: John Wiley & Sons, pp 883.

Shepard, F.P. 1976. Coastal classification and changing coastlines, Geosciences and Man, 14, 53-64.

Shepard, F. P. 1977. Geological Oceanography, New York, NY: Crane, Rusak, & Company.

Simpson, J. H. 1998: Tidal processes in shelf seas. In "The Sea", Vol. 10, A.R. Robinson and K.H. Brink, eds., Wiley, New York, Chapter 5, pp. 113-150.

UK Hydrographic Office, 2006. Admiralty TotalTide, Somerset, UK: The United Kingdom Hydrographic Office**.**

Visual Learning Systems, Feature Analyst 4.1 for ArcGIS: Training Guide, Missoula, Montana: Visual Learning Systems, Inc.

GLOSSARY OF TERMS AND DEFINITIONS

Introduction. This glossary only provides terms that are useful for the description of coastal phenomena discussed in this progress report. Many shallow water processes impact military operations. Some of these terms and descriptions relate to information that should be considered during the rapid response planning process and incorporated into presentations to the Crisis Action Team during mission analysis.

accretion — The gradual or imperceptible buildup of land by natural or artificial forces, as on a beach by water or airborne deposition of sediment particles, or on a flood plain by the accumulation of sediment deposited by a river or stream. Artificial accretion includes deposition associated with engineering activities, such as bulkheads, groins, breakwaters, or beach fill.

air gap — Vertical gap or clearance separating the sea surface from the lowest portion on the deck of a bridge.

alongshore — Parallel to and near the shoreline or coast, such as an "alongshore drift" or "alongshore current".

apogean tides — Tides of decreased range occurring monthly as a result of the Moon in apogee.

apogee — The point in the Moon's orbit that is farthest from the Earth.

attribute — Descriptive characteristic or quality of a feature. Attributes may be represented by locational or non-locational descriptive information about a feature.

backshore — The upper or inner, usually dry, zone of the shore or beach, lying between the high-water line of mean spring tides and the upper limit of shore-zone processes; it is acted upon by waves or covered by water only during exceptionally severe storms or unusually high tides. It is essentially horizontal or slopes gently landward, and is divided from the foreshore by the crest of the most seaward berm.

bar — A generic term for any of various elongated offshore ridges, banks, or mounds of sand, gravel, or other unconsolidated material, submerged at least at high tide, and built up by the action of waves or currents on the water bottom, especially at the mouth of a river or estuary, or at a slight distance from the beach.

barrier island — A long, narrow coastal sandy island, representing a broadened barrier beach that is above high tide and parallel to the shore, and that commonly has dunes, vegetated zones, and swampy terrains.

beach — The unconsolidated material that covers a gently sloping zone, typically with a straight, convex, or concave profile, extending landward from the low-water line to the place where there is a definite change in material or physiographic form (such as a bluff), or to the line of permanent vegetation (usually the effective limit of the highest storm waves). A beach includes a foreshore and backshore.

beach profile — A cross-section taken perpendicular to a given beach contour; the profile may include the face of a dune or sea wall, extend over the backshore, across the foreshore, and seaward underwater into the nearshore zone.

channel — A natural or artificial waterway of perceptible extent which either periodically or continuously contains moving water, or which forms a connecting link between two bodies of water.

class — A set of pixels in a GIS or image file that represents areas that have the same

attribute or share the same condition.

classification — Process of assigning individual observations of features into groups, categories, or classes.

coast — A strip of land of indefinite width (may be several kilometers) that extends from the shoreline inland to the first major change in terrain features.

constituent — One of the harmonic elements in a mathematical expression for the tide-producing force and in corresponding formulas for the tide or tidal current. Each constituent represents a periodic change or variation in the relative positions of the Earth, Moon, and Sun.

concave beach — A crescent-shaped beach, between two headlands which is also called a pocket beach. In an idealized setting, there is very little or no exchange of sediment between the pocket beach and the adjacent shorelines.

convex beach — A beach that is usually associated with an area of higher elevation, more resistant to erosion than surrounding areas, and less susceptible to flooding. The headland supplies sand and gravel to the beach.

cross-shore — Perpendicular to the shoreline.

current — A horizontal movement or continuous flow of water in a given direction with a more or less uniform velocity, producing a perceptible mass transport, set in motion by winds, waves, tides, gravity, or differences in temperature and density, and of a permanent or seasonal nature.

datum — Any numerical or geometric quantity or value that serves as a base or reference for other quantities or values.

delta — The low, nearly flat, alluvial tract of land at or near the mouth of a river, commonly forming a triangular or fan-shaped plain of considerable area, crossed by many distributaries of the main river, perhaps extending beyond the general trend of the coast, and resulting from the accumulation of sediment supplied by the river in such quantities that it is not removed by tides, waves, and currents. Most deltas are partly subaerial and partly below water.

deposition — The laying, placing, or throwing down of any material; specifically, the constructive process of accumulation into beds, veins, or irregular masses of any kind of loose rock material by any natural agent, such as the mechanical settling of sediment from suspension in water, the chemical precipitation of mineral matter by evaporation from solution, or the accumulation of organic material on the death of plants and animals.

Digital Elevation Model — A digital representation of a continuous variable over a two-dimensional surface by a regular array of z values referenced to a common datum.

diurnal — Having a period or cycle of approximately one tidal day.

diurnal tide — One high water and one low water occurring during a tidal day (24.84 hours). A single flood and a single ebb period of a reversing current during a tidal day.

ebb current — The movement of a tidal current away from shore or down a tidal stream.

erosion — The general process or the group of processes whereby the materials of the Earth's crust are loosened, dissolved, or worn away, and simultaneously moved from one place to another, by natural agents, which include weathering, solution, corrosion, and transportation, but usually exclude mass wasting; specifically, the mechanical destruction of the land and the removal of material (such as soil) by running water (including rainfall), waves and currents, moving ice, or wind.

estuary — The seaward end or the widened funnel-shaped tidal mouth of a river valley

where fresh water comes into contact with seawater and where tidal effects are evident (e.g., a tidal river, or a partially enclosed coastal body of water where the tide meets the current of a river).

feature — A geographic component of the earth's surface that has both spatial and attribute data associated with it (e.g. river, shoreline, and road).

fetch — The distance of uninterrupted water surface over which the wind has blown to form waves. Longer fetch means higher energy waves.

fjord — Very deep U-shaped estuaries formed by the drowning of glaciated valleys on the Western side of land masses in temperate latitudes.

flood current — The horizontal movement of a tidal current toward the shore or up a tidal river or estuary.

geo-rectify — The process by which an image or grid is converted from image coordinates to map coordinates.

GIS — A geographic information System composed of computer hardware, software, and procedures designed to support the capture, management, manipulation, analysis, modeling, and display of spatially referenced data for solving complex planning and management problems.

gradient — The degree of inclination to the horizontal. Gradients and slopes are usually expressed as a ratio, such as 1:25, indicating one unit rise in 25 units of horizontal distance; or in a decimal fraction (0.04).

groin — A narrow, elongated structure extending seaward perpendicular from the beach to trap longshore drift and build up a section of beach.

harmonic analysis — The mathematical process by which the observed tide or tidal current at any place is separated into basic harmonic constituents.

high energy coast — Coasts in which wave power is strong for a significant part of the year (e.g. Alaska to Iceland and Chile).

hyperspectral — Collection and analysis of many narrow bands in the electromagnetic spectrum.

jetty — A narrow, elongated structure built perpendicular to the shoreline at coastal inlets to prevent longshore drift from filling the inlet and providing protection for navigation.

longshore drift — Movement of sediments approximately parallel to the shore.

low energy coast — Coasts in which wave power is weaker, low fetch, few gales enclosed and therefore sheltered (e.g. Mediterranean and Baltic Seas).

monsoon — Winds caused by much greater annual variation of temperature over large land areas compared with neighboring ocean surfaces, causing an excess of pressure over the continents in winter and a deficit in summer. Monsoons are the strongest on the southern and eastern sides of Asia.

mangrove coast — Coastal region populated by tropical evergreen trees and shrubs with stilt like roots and stems forming dense thickets along the shore.

maximum cross correlation — A satellite feature tracking method requiring the analyst to compute the cross-correlation coefficients of some surface feature between templates in the first image and all their corresponding identically sized templates within a larger "search window" in the second image.

mixed tide — A tide that presents a large inequality in either the high or low water heights with two high waters and two low waters usually occurring each tidal day.

morphodynamics — The mutual interaction and adjustment of the seafloor topography and

fluid dynamics involving the motion of sediment.

mudflat — A muddy, low-lying strip of ground by the shore, or an island, usually submerged more or less completely by the rise of the tide.

multispectral — Is the ability of a remote sensing device to detect electromagnetic energy in at least two or more individual wavelength intervals.

neap tide — A tide of decreased range occurring semimonthly as the result of the moon being in quadrature.

nearshore — The region extending from the swash zone to the position marking the start of the offshore zone, typically at water depths on the order of 20 m.

offshore — The region beyond the nearshore zone where sediment motion induced by waves alone effectively ceases and where the influence of the seabed on wave action is small in comparison with the effect of wind.

prediction — The determination of what might happen in the future. Tide predictions are predetermined times and heights of high or low water at a reference station.

quality control — Analysis products and procedures that are used to ensure the project conforms to requirements, specifications, and working standards.

sandbar — An accretionary feature that impedes the flow of water.

sea breeze — A coastal local wind that blows from sea to land, caused by the temperature difference when the sea surface is colder than the adjacent land.

sediment — Unconsolidated solid material that comes from weathering of rock and is carried by, suspended in, or deposited by water or wind.

semidiurnal tide — Two high waters and two low waters each tidal day. Two flood and two ebb periods each day.

shapefile — An GIS data set used to represent a set of geographic features such as groins, waterlines, and mudflat locations. Shapefiles can represent point, line, or area features. Each feature in a shapefile represents a single geographic feature and its attributes.

shifting channel — Changing natural or artificial watercourses, with a definite bed and banks to confine and conduct continuously or periodically flowing water.

shoal — Shallow water obstacle, such as a sandbar.

shoreline — The land-water boundary referenced to a tidal datum such as Mean Higher High Water.

shore protection — Reinforcement of the shore with bulkheads/seawalls, breakwaters, groins, revetments, and jetties.

spring tide — Particularly high or low tides caused when the Sun, Moon and Earth all lie in a straight line, which happens twice a month.

straight beach — Linear beach indicating a balance among waves, winds, and erosion.

surf zone — The zone of wave action from the waterline out to where the waves start to break as surf.

tidal current — A horizontal movement of the water caused by gravitational interactions between the Sun, Moon, and Earth.

tidal datum — A base elevation based on the phase of the tide and used as a reference to determine heights or depths.

tide — The periodic rise and fall of the water resulting from gravitational interactions between the Sun, Moon, and Earth.

waterline — The instantaneous land-water boundary at the time of imaging process.

ANNOTATED BIBLIOGRAPHY

Introduction. This list of books and journal articles is followed by a brief (usually about 100 words) descriptive and evaluative paragraph, which serves as the annotation. The purpose of the annotation is to inform the reader of the relevance, accuracy, and quality of material that is relevant to this project. This is an update from Naval Research Laboratory Memorandum Report, NRL/MR/7205—04-8837.

Choi, K.S., R.W. Dalrymple, S.S. Chun, and S.-P. Kim, 2004. Sedimontology of Modern, Inclined Heterolithic Stratification (IHS) in the Macrotidal Han River delta, Korea. Journal of Sedimentary Research, 74(5): 677 - 689.

Stratification of sediments is analyzed on the macrotidal (tidal range 3.6--7.8 m), Han River delta. Muds are approximately 25 m thick. The investigated channel was ebb dominated. Seasonal discharge variations of the Han River are not obvious in the deposits owing to the energetic tidal environment of the studied channel.

Fonstadt, M.A. and W.A. Marcus, 2005. Remote sensing of stream depths with hydraulically assisted bathymetry (HAB) models. Geomorphology, 72, pp. 320-339.

Remote sensing imagery and open channel flow algorithms are used to estimate depths from imagery of the Brazos River in Texas and Lamar River in Wyoming. Key hydrodynamic parameters used in simple models were discharge, average velocity, hydraulic radius, wetted perimeter, and depth. Formulas included the discharge and Manning equations. Remote sensing parameters of importance were intensity, diffuse attenuation coefficient, digital number value, and distance value. The Beer-Lambert Law was applied to determine discharge. An iterative approach is recommended to determine depths by minimizing the difference between estimated and measured discharge.

Nina, G., V. Nekrutkin, A. Zhigljavsky, *Analysis of Time Series Structure: SSA and related Techniques*, London, United Kingdom: Chapman & Hall/CRC, 2001

A statistical approach suited for nonlinear physics and signal processing where a time series is broken into a sum of smaller components such as a trend. The technique relies on being able to separate the signal into numerous components. SSA software forms a series into a trajectory matrix, decomposes the trajectory matrix into bi-orthogonal matrices, reconstructs the matrix as a sum of resultant matrices, and then transfers each resultant matrix into a time series.

Niedermeier, A., D. Hoja, and S. Lehner. 2005. Topography and morphodynamics in the German Bight using SAR and optical remote sensing data, Ocean Dynamics. 55, pp 100-109.

Satellite data from optical and radar sensors is used to build digital elevation models of the Wadden Sea, which includes the salt marshes, islands, and dunes located on the North Sea. Discussions describe waterline methodology to assess morphodynamic changes in bottom topography and interpolation of waterlines. Important concepts in this paper relate to

edge detection and the application of wavelets.

Park, K. J.-H. Oh, H.-S. Kim, and H.-H Im. 2002. Case Study: Mass Transport Mechanism in Kyunggi Bay around Han River Mouth, Korea, Journal of Hydraulic Engineering, 128(3), pp. 257-267

   Application of POM forced by the M_2, S_2, K_1, and O_1 tides was adapted to also include the salt balance equation, heat-balance equation, and wetting and drying. Macrotidal tide ranges of 7.9 and 3.5 m during neap and spring tides were reported. Investigations focused on nontidal forces such as freshwater discharge. Ebb discharges are reported to be from 1.26 to 2.71 m^2/s

Park, Y.C., H.J. Lee, D.W. Kim, M.Y. Lee, 2004. Nutrient dynamics and short-time scale variability of environmental parameters during the tidal cycle in the coastal waters of Incheon, Korea, MTS/IEEE OCEANS '04, Volume 3, pp 1281 – 1283.

   Water properties such as nutrients, dissolved oxygen, and turbidity vary with the tidal cycle at the lower part of Han River Estuary, Korea. Real time data was available from an automated monitoring system that included a nutrient autoanalyzer and an acoustic Doppler current profiler. The tidal cycle was reported to be asymmetry and maximum tidal velocity was reported to be 1.8m/s with 9.2m of tidal range.

Park, Y.-H., K.-S. Lee, H.-Y. Lee, I. Son, J.-R., Lee (ed.), *Atlas of Korea,* Seoul, Republic of Korea: Sung Ji Mun Hwa Co Ltd, 2000.

   This atlas describes the geography of the Korean peninsula in English. There are maps and tables providing climate, soil, vegetation, agriculture, forestry, fishery, mining, foreign trade, manufacturing, population, transportation, commerce, tourism, medicine, and education data. Relief is shown on maps by contours, shading, and spot heights.

Ryu, J.H., W.J. Cho, and J.S. Won. Estimation of the sedimentation budget in tidal flat using remotely sensed data. 2001. Proceedings IGARSS, Sydney, Australia, pp. 2409-2411.

   The analysis of mudflats using specific band ratios for edge detection to build intertidal DEMs is discussed. Visible and panchromatic bands were not used due to high turbidity. The edge detection was accomplished by taking (TM 4 – TM 3) / (TM 4 + TM 3). Slopes of the mudflats are less then 0.09°. Tidal currents were reported to be on the order of 1.5 m/s during ebbs and 1.15 m/s during floods. The resultant DEM was used to assess the sediment budget and to study major intertidal channels.

Ryu, J.H., W.J. Cho, and J.S. Won. A study on the geomorphological change in tidal-flat using multisource remotely sensed data: A case study in the Gomso Bay, Korea. 2000. Proceedings of IGARSS, Hawaii, USA, pp. 1892-1894.

   Detection and measurement of terrain and surface sediment changes for tidal flats was

addressed. The study area had a semidiurnal tide with a range of 4.3 m. It is assumed that terrain variations in tidal flats are insignificant over short time periods relating to images and that measurements of tide conditions are available from the Korea Ministry of Maritime Affairs and Fisheries.

Toril, K., T. Hoshi, T. Kano, B.J. Cho, B.H. Lim, and M.S. Choi, 1996. Investigation on tidal land reclamation in Korea using satellite image data, Proceeding of the 17th Asian Conference on Remote Sensing, 4-8 November 1996, Sri Lanka, 6 pp.

Time series of satellite imagery were compiled to monitor coastal changes resulting from large-scale land improvements along the western coast of South Korea. Land consolidation and irrigation systems in Mokpo and Kunsan are highlighted and new construction is described. This particular report highlights land reclamation efforts that change the hydrodynamic patterns of the region.

Won, J.-S., S.-H. Hong, M.-K. Kim, 2005. Application of ERS SAR to the Study of Korean Tidal Flats, Geoscience and Remote Sensing Symposium, 25-29 July 2005, Proceedings of IGARSS '05, Volume 8, pp 5683–5686.

Important factors in remote sensing of mud flats are surface roughness, interstitial water content of exposed bottom, and remnant surface water. Tidal conditions must be considered in imagery analysis.

Won, J.-S. and J.-H. Ryu. 2002. Control Factors of Spectral Reflectance in Tidal Flat: A Case Study in the Gomso Bay, Korea, Proceedings of IGARSS, Toronto, Canada, pp 1588-1590.

Tidal conditions are considered as a major factor in spectral reflectance. The effective exposed area is (total area – water cover) / total area. Spectral reflectance is measured using a field spectrometer. Critical grain sizes governing moisture content in a tidal flat are ~ 0.25 mm.

Won, J.-S. and Y.-H. Na, and S.-W. Kim, 2003. Tidal Flat DEM Generation by Satellite Remote Sensing. Geoscience and Remote Sensing Symposium, IGARSS '03, 21-25 July 2003, Volume 3, pp 2116-2118.
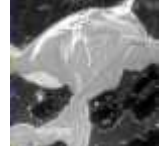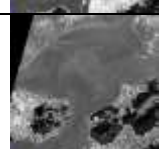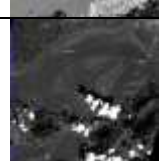
A high precision digital elevation model (DEM) in tidal flat is valuable for coastal erosion monitoring. To monitor active coastal changes, a DEM having an accuracy of better than 20 cm is required. The waterline method using optic images and space-borne radar interferometry were tested at tidal flats located in Gomso Bay and Saemangeum. Band selection was critical for the waterline method especially on the ebb tide, and near infrared was superior to short wavelength infrared. The accuracies of the estimated DEMs were 10.9 cm and 9.8 cm at Gomso Bay and the Saemangeum tidal flat, respectively.

Yoo, H.-R., I.-H. Bae, J.-H. Ryu, and Y.-H. Ahn, 2005. A Study of the Sedimentary Environments in the Korean Tidal Flat Using Landsat TM/ETM+, Kompsat EOC, and IKONOS, Geoscience and Remote Sensing Symposium, IGARSS '05, 25-29 July 2005, Proceedings, 2005 IEEE International Volume 1, pp 431-433.

Observation and discussion of changes in tidal flats (Kanghwa and Hwang-Do) and coastal areas. The Kanghwa tidal flat is one of the biggest flats on the west coast of Korea. Tidal flats are characterized as open and closed types or as mud, sand, and mixed flats. Tide gage data was considered to be essential in referencing extracted waterlines.

Listing of Available Imagery

Thumbnail	Filename (.tif unless stated) [Shapefile (if exists)]	Size (KB)	Sensor	Date/UTC (YYYYMMDD) (HH:MM:SS)	Mode Angle
	S119870131T023618_HRE_15mPAN [_shoreline.shp]	1121	SPOT 1	19870131 02:36:18	PAN 7.3
	L419890517T014408_HRE_15mMSI [_shoreline.shp]	6722	Landsat4	19890517 01:14:08	MSI Nadir
	S219901022T023326_HRE_15mPAN [_shoreline.shp]	1121	SPOT 2	19901022 02:33:26	PAN 2.2
	L519910531T013330_HRE_15mMSI [_shoreline.shp]	6722	Landsat5	19910531 01:33:30	MSI Nadir
	L519911022T013438_HRE_15mMSI [_multiclass shoreline.shp]	6722	Landsat5	19911022 01:34:38	MSI Nadir
	S219911022T021429_HRE_15mPAN [_shoreline.shp]	1121	SPOT 2	19911022 02:14:29	PAN -26.9
	S219931019T021334_HRE_15mPAN [_shoreline.shp]	1121	SPOT 2	19931019 02:13:34	PAN 2.2
	S219931203T024744_HRE_15mPAN [_shoreline.shp]	1121	SPOT 2	19931203 02:47:44	PAN
	S319940107T023248_HRE_15mPAN [_shoreline.shp]	1121	SPOT 3	19940107 02:32:48	PAN
	S219940519T022636_HRE_15mPAN [_land.shp] (no waterlines)	1121	SPOT 2	19940519 02:26:36	PAN

	S319940723T024411_HRE_15mPAN [_shoreline.shp]	1121	SPOT 3	19940723 02:44:11	PAN 19.9
	S319940724T022453_HRE_15mPAN [_shoreline.shp]	1121	SPOT 3	19940724 02:24:53	PAN -11.4
	S319941104T024338_HRE_15mPAN [_shoreline.shp]	1121	SPOT 3	19941104 02:43:38	PAN 20.3
	S319950216T024239_HRE_15mPAN [_shoreline.shp]	1121	SPOT 3	19950216 02:42:39	PAN 21.6
	S319950601T022422_HRE_15mPAN [_shoreline.shp]	1121	SPOT 3	19950601 02:24:22	PAN -11.0
	S319951025T021730_HRE_15mPAN [_shoreline.shp]	1121	SPOT 3	19951025 02:17:30	PAN -22.0
	S319960206T021723_HRE_15mPAN [_shoreline.shp]	1121	SPOT 3	19960206 02:17:23	PAN
	S319960921T023053_HRE_15mPAN [_shoreline.shp]	1121	SPOT 3	19960921 02:30:53	PAN 3.2
	S319960927T021532_HRE_15mPAN [_shoreline.shp]	1121	SPOT 3	19960927 02:15:32	PAN -24.4
	S219971231T021354_HRE_15mPAN [_shoreline.shp]	1121	SPOT 2	19971231 02:13:54	PAN -27.5
	S119980409T023825_HRE_15mPAN [_shoreline.shp]	1121	SPOT 1	19980409 02:38:25	PAN

	S219980428T024235_HRE_15mPAN [_shoreline.shp]	1121	SPOT 2	19980428 02:42:35	PAN 19.2
	S119981023T025228_HRE_15mPAN [_shoreline.shp]	1121	SPOT 1	19981023 02:52:28	PAN 30.0
	S419990101T024859_HRE_15mMSI [_shoreline.shp]	4481	SPOT 4	19990101 02:48:59	MSI 24.7
	L719990630T020330_HRE_15mMSI [_shoreline.shp]	6722	Landsat7	19990630 02:03:30	MSI Nadir
	L719991207T020343_HRE_15mPAN [_shoreline1.shp]	1121	Landsat7	19991207 02:03:43	PAN Nadir
	L720000124T020337_HRE_15mMSI [_shoreline.shp]	6722	Landsat7	20000124 02:03:37	MSI Nadir
	L720000429T020308_HRE_15mMSI [_shoreline.shp]	6722	Landsat7	20000429 02:03:08	MSI Nadir
	L720000429T020308_HRE_15mPAN [_shoreline1.shp]	1121	Landsat7	20000429 02:03:08	PAN Nadir
	L720000904T020138_HRE_15mMSI [_shoreline.shp]	6722	Landsat7	20000904 02:01:38	MSI Nadir
	L720000904T020138_HRE_15mPAN	1121	Landsat7	20000904 02:01:38	PAN Nadir
	AS20000904T024324_HRE_15mMSI. dat [_shoreline.shp]	13342	ASTER	20000904 02:43:24	MSI Nadir

	L720010110T020117_HRE_15mMSI [_shoreline.shp]	6722	Landsat7	20010110 02:01:17	MSI Nadir
	L720010211T020114_HRE_15mMSI [_shoreline.shp]	6722	Landsat7	20010211 02:01:14	MSI Nadir
	L720010211T020114_HRE_15mPAN	1121	Landsat7	20010211 02:01:14	PAN Nadir
	L720010315T020106_HRE_15mMSI [_shoreline.shp]	6722	Landsat7	20010315 02:01:06	MSI Nadir
	L720010603T020031_HRE_15mMSI [_shoreline.shp]	6722	Landsat7	20010603 02:00:31	MSI Nadir
	L720010622T020031_HRE_15mMSI [_shoreline.shp]	6722	Landsat7	20010622 02:00:31	MSI Nadir
	L720010822T015937_HRE_15mPAN [_shoreline.shp]	1121	Landsat7	20010822 01:59:37	PAN Nadir
	L720010923T015917_HRE_15mMSI [_shoreline.shp]	6722	Landsat7	20010923 01:59:17	MSI Nadir
	L720011110T015916_HRE_15mMSI [_shoreline.shp]	6722	Landsat7	20011110 01:59:16	MSI Nadir
	L720011228T015925_HRE_15mMSI [_shoreline.shp]	6722	Landsat7	20011228 01:59:25	MSI Nadir
	L720020129T015936_HRE_15mPAN [_shoreline.shp]	1121	Landsat7	20020129 01:59:36	PAN Nadir

L720020403T015934_HRE_15mMSI [_shoreline.shp]	6722	Landsat7	20020403 01:59:34	MSI Nadir
AS20020426T023605_HRE_15mMSI. dat [_shoreline.shp]	13342	ASTER	20020426 02:36:05	MSI Nadir
L720020606T015925_HRE_15mMSI [_shoreline.shp]	6722	Landsat7	20020606 01:59:25	MSI Nadir
L720020910T015836_HRE_15mMSI [542_shoreline.shp]	6722	Landsat7	20020910 01:58:36	MSI Nadir
AS20020917T023603_HRE_15mMSI. dat [_shoreline.shp]	13342	ASTER	20020917 02:36:03	MSI Nadir
L720021028T015934_HRE_15mMSI [542_shoreline.shp]	6722	Landsat7	20021028 01:59:34	MSI Nadir
L720021231T015910_HRE_15mMSI [_shoreline.shp]	6722	Landsat7	20021231 01:59:10	MSI Nadir
L720030201T015922_HRE_15mMSI [_shoreline.shp]	6722	Landsat7	20030201 01:59:22	MSI Nadir
L720030406T015934_HRE_15mMSI [_shoreline.shp]	6722	Landsat7	20030406 01:59:34	MSI Nadir
AS20030406T022905_HRE_15mMSI. dat [_shoreline.shp]	13342	ASTER	20030406 02:29:05	MSI Nadir
L720030508T015934_HRE_15mMSI [_shoreline.shp]	6722	Landsat7	20030508 01:59:34	MSI Nadir

	AS20031006T023425_HRE_15mMSI.dat [_shoreline.shp]	13342	ASTER	20031006 02:34:25	MSI Nadir
	AS20031022T023432_HRE_15mMSI.dat [_shoreline.shp]	13342	ASTER	20031022 02:34:32	MSI Nadir
	S520031221T021750_HRE_15mMSI [_shoreline.shp]	4481	SPOT 5	20031221 02:17:50	MSI 24.0
	QB20051017T024732_HRE_15mMSI [_shoreline.shp]	8929	Quickbird	20051017 02:47:32	MSI
	QB20051017T024732_HRE_4MSI_RMP.dat [_shoreline.shp]	125000	Quickbird	20051017 02:47:32	MSI (4m Res)
	QB20051025T023744_HRE_15mMSI [_shoreline.shp]	8929	Quickbird	20051025 02:37:44	MSI
	QB20051030T024250_HRE_15mMSI [_shoreline.shp]	8929	Quickbird	20051030 02:42:50	MSI
	QB20051104T024815_HRE_4MSI.dat [_shoreline.shp]	210473	Quickbird	20051104 02:48:15	MSI (4m Res)
	QB20060331T023917_HRE_15mMSI [_shoreline.shp]	8929	Quickbird	20060331 02:39:17	MSI
	QB20060405T024421_HRE_15mMSI [_shoreline.shp]	8929	Quickbird	20060405 02:44:21	MSI
	QB20060405T024421_HRE_4MSI.dat [template_shoreline.dat]	163543	Quickbird	20060405 02:44:21	MSI (4m Res)

|	QB20060428T025039_HRE_15mMSI [_shoreline.shp]	8929	Quickbird	20060428 02:50:39	MSI

SIMULATED TIME SERIES FROM REMOTE SENSING IMAGERY

Introduction

The overarching goal of this study involves the prediction of tides utilizing imagery derived information. The most important task involves obtaining water level elevations by estimating depths by crossing extracted imagery shorelines with transects orthogonal to the mean lower low water (MLLW) shoreline depicted on a high-resolution digital elevation model. This effort is still underway utilizing semi-automated feature extraction algorithms. Estimates of depths seaward of the MLLW datum will be made using a combination of equilibrium beach profiles, shallow-water reflectance models, and wave kinematics.

Harmonic analysis techniques will be used to predict tides at locations where water level fluctuations may be derived. A synthetic data set of imagery derived water levels has been developed to practice several techniques that result in building a continuous tidal time series from inconsistent data. The practice time series has been generated as input for a customized harmonic analysis application. Times for the listed elevations were obtained from a variety of satellite images. The elevations were predictions based on Station Number 7480 in Oep'ori in the Republic of Korea.   The mean high water spring range is 8.2 m and the mean low water spring is 1.0 m. Mean Sea Level (MSL) at this secondary harmonic station is 4.57 m. Figure D-1 depicts this time series.

HRE Predicted Water Levels
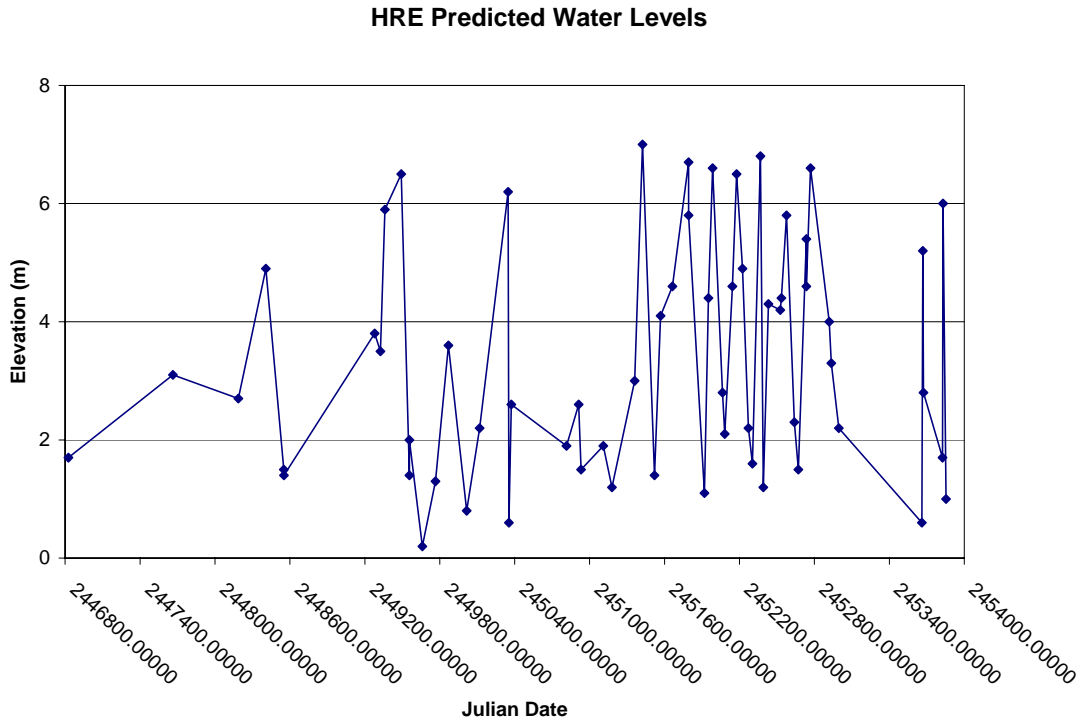
Figure D-1. Predicted Oep'ori water levels. Each data point represents the time of imaging from commercial satellites.

The HRE is the broad and lower portion of the Han River which flows through Seoul (37º 32' N, 127º 00' E) before emptying into the Yellow Sea. The river is more than 1 km wide as it meanders through Seoul. A primary tidal station is located in Incheon which is approximately 38 km from Seoul. Standard time is UTC plus 9 hours. There is no daylight saving time in Republic of Korea. The secondary harmonic port at Total Tide Station Number 7480, Oep'ori was used to predict water levels and compute % Mean High Water Spring (MHWS). Datum information from Total Tides is MHWS 8.2 m, MHWN 6.0 m, MSL 4.57 m, MLWN 3.1 m, and MLWS 1.0 m. Oep'ori is located on the west coast of Ganghwa Island. The predictions are provided in Table D-1.

Table D-1. Simulated Time Series. The listed water level fluctuations will be used to practice Singular Spectrum Analysis or harmonic analysis techniques useful in predicting tides. This time series is similar to the one being derived from imagery comparisons to a digital elevation model. Results will be described in the final report.

YR	MON	DY	HR (UTC)	MIN	JULIAN (DY of YR)	ELEV (M)	STAGE	% MHWS
1987	Jan	31	02	36	31.1083	1.7	Falling	20.7
1989	May	17	01	44	137.0722	3.1	Rising	37.8
1990	Oct	22	02	33	295.1063	2.7	Falling	32.9
1991	May	31	01	33	151.0646	4.9	Falling	59.7
1991	Oct	22	01	34	295.0653	1.5	Falling	18.3
1991	Oct	22	02	14	295.0931	1.4	Rising	17.1
1993	Oct	19	02	13	292.0924	3.8	Falling	46.3
1993	Dec	03	02	47	337.1160	3.5	Falling	42.7
1994	Jan	07	02	32	7.1056	5.9	Rising	72.0
1994	May	19	02	26	139.1014	6.5	Rising	79.3
1994	Jul	23	02	44	204.1139	1.4	Falling	17.1
1994	Jul	24	02	24	205.1000	2.0	Falling	24.4
1994	Nov	04	02	43	308.1132	0.2	Rising	2.4
1995	Feb	16	02	42	47.1125	1.3	Falling	15.8
1995	Jun	01	02	24	152.1000	3.6	Falling	43.9
1995	Oct	25	02	17	298.0951	0.8	Falling	9.7
1996	Feb	06	02	17	37.0951	2.2	Falling	26.8
1996	Sep	21	02	30	265.1042	6.2	Falling	75.6
1996	Sep	27	02	15	271.0938	0.6	Falling	7.3
1996	Oct	16	02	50	290.1181	2.6	Falling	31.7
1997	Dec	31	12	13	365.0924	1.9	Falling	23.2
1998	Apr	09	02	38	99.1097	2.6	Rising	31.7
1998	Apr	28	02	42	118.1125	1.5	Falling	18.3
1998	Oct	23	02	52	296.1194	1.9	Falling	23.2
1999	Jan	01	02	48	1.1167	1.2	Rising	14.6
1999	Jun	30	02	03	181.0854	3.0	Falling	36.6
1999	Sep	02	02	03	245.0854	7.0	Falling	85.4
1999	Dec	07	02	03	341.0854	1.4	Falling	17.1
2000	Jan	24	02	03	24.0854	4.1	Falling	5.0

2000	Apr	29	02	03	120.0854	4.6	Rising	56.1
2000	Sep	04	02	01	248.0840	6.7	Falling	81.7
2000	Sep	04	02	43	248.1132	5.8	Falling	70.7
2001	Jan	10	02	01	10.0850	1.1	Falling	13.4
2001	Feb	11	02	01	42.0850	4.4	Falling	53.7
2001	Mar	15	02	01	74.0850	6.6	Falling	80.5
2001	Jun	03	02	00	154.0833	2.8	Rising	34.1
2001	Jun	22	02	00	174.0833	2.1	Falling	25.6
2001	Aug	22	01	59	234.0826	4.6	Falling	56.1
2001	Sep	23	01	59	266.0826	6.5	Falling	79.2
2001	Nov	10	01	59	314.0826	4.9	Rising	59.8
2001	Dec	28	01	59	362.0826	2.2	Rising	26.8
2002	Jan	29	01	59	29.0826	1.6	Falling	19.5
2002	Apr	03	01	59	93.0826	6.8	Falling	82.9
2002	Apr	26	02	36	116.1083	1.2	Rising	14.6
2002	Jun	06	01	59	157.0826	4.3	Rising	52.4
2002	Sep	10	01	58	253.0819	4.2	Falling	51.2
2002	Sep	17	02	36	260.1083	4.4	Rising	53.6
2002	Oct	28	01	59	301.0826	5.8	Falling	70.7
2002	Dec	31	01	59	365.0826	2.3	Rising	28.0
2003	Feb	01	01	59	32.0826	1.5	Falling	18.3
2003	Apr	06	01	59	96.0826	5.4	Falling	65.9
2003	Apr	06	02	29	96.1035	4.6	Falling	56.1
2003	May	08	01	59	128.0826	6.6	Falling	80.5
2003	Oct	06	02	34	279.1069	4.0	Rising	48.8
2003	Oct	22	02	34	295.1069	3.3	Rising	40.2
2003	Dec	21	02	17	355.0951	2.2	Rising	26.8
2005	Oct	17	02	47	290.1160	0.6	Rising	7.3
2005	Oct	25	02	37	298.1090	5.2	Falling	63.4
2005	Oct	30	02	42	303.1125	2.8	Rising	1.0
2006	Mar	31	02	39	90.1104	1.7	Falling	20.7
2006	Apr	05	02	44	95.1139	6.0	Falling	73.2
2006	Apr	28	02	50	118.1181	1.0	Falling	12.2

Times correspond to disparate commercial imagery holdings for HRE at NRL-DC.

COAST TYPES

Introduction

As mentioned by NRL (1995) and McDermid et al. (1997), the littoral battlespace has spatially and temporally changing METOC processes caused by complex interactions of land, shallow water, and atmosphere. A littoral classification system could be based on the magnitude of generalized forces attributed to shoreline shape and coastal features. In addition, the above references used the Comprehensive Ocean and Atmospheric Data Set or COADS along with selected imagery as a starting point to characterize waves for several important areas for the EFV. Researchers can use this type of global data to develop answers on a range of topics that depend on descriptive statistics or modeling with authoritative input values.

COADS is useful in understanding climate variability. Data and information from COADS are frequently used to calibrate climate models. Today, COADS is known as the International Comprehensive Ocean-Atmosphere Data Set (ICOADS). It provides global marine observations from 1784 to 2004 from ships of opportunity that have been collecting, editing, and summarizing parameters of importance such as temperatures, humidity, winds, pressures, waves, and clouds. This information could be used to develop a hierarchical littoral classification system that generalizes the physical and biological processes attributed to shoreline shape and coastal features. ICOADS provides a basis for safe engineering and operations of amphibious craft.

As a simple example, Shepard (1976, 1977) has categorized coasts into 11 distinct classifications (see Figure E-1). A hierarchical system might evaluate subcomponents (levels 2, 3, and 4) that are the dominant characteristics of the level 1 coast type. Selected geospatial elements could be analyzed from imagery stacks and databases such as ICOADS to better characterize a particular area of responsibility.

Level 1. Coast type (estuary, mangrove, coral, barrier island, wave-cut cliff, etc.)

Level 2. Offshore approaches (hydrodynamic conditions – tides, currents, surf, distance between low and high water marks, water temperature, salinity, bottom characteristics, gradients, ambient noise, etc.)

Level 3. Shore (beach shape, berm, beach composition, bearing strength, trafficability, structures, seaports, etc.)

Level 4. Exits Inland (cliffs, bluffs, dunes, terraces, promontories, pinnacles, grottoes, caves, and caverns, marshes, swamps, forests, cities, towns, villages, roads, airfields, landing zones, etc.)

Based on HALE progress, a well thought out littoral classification system would enable analysts to use waterlines, DEMs, and beach profiles to make an educated assessment on

the location of the 6-meter curve. This feature is required for EFV transition from a planing hull to a tractor.
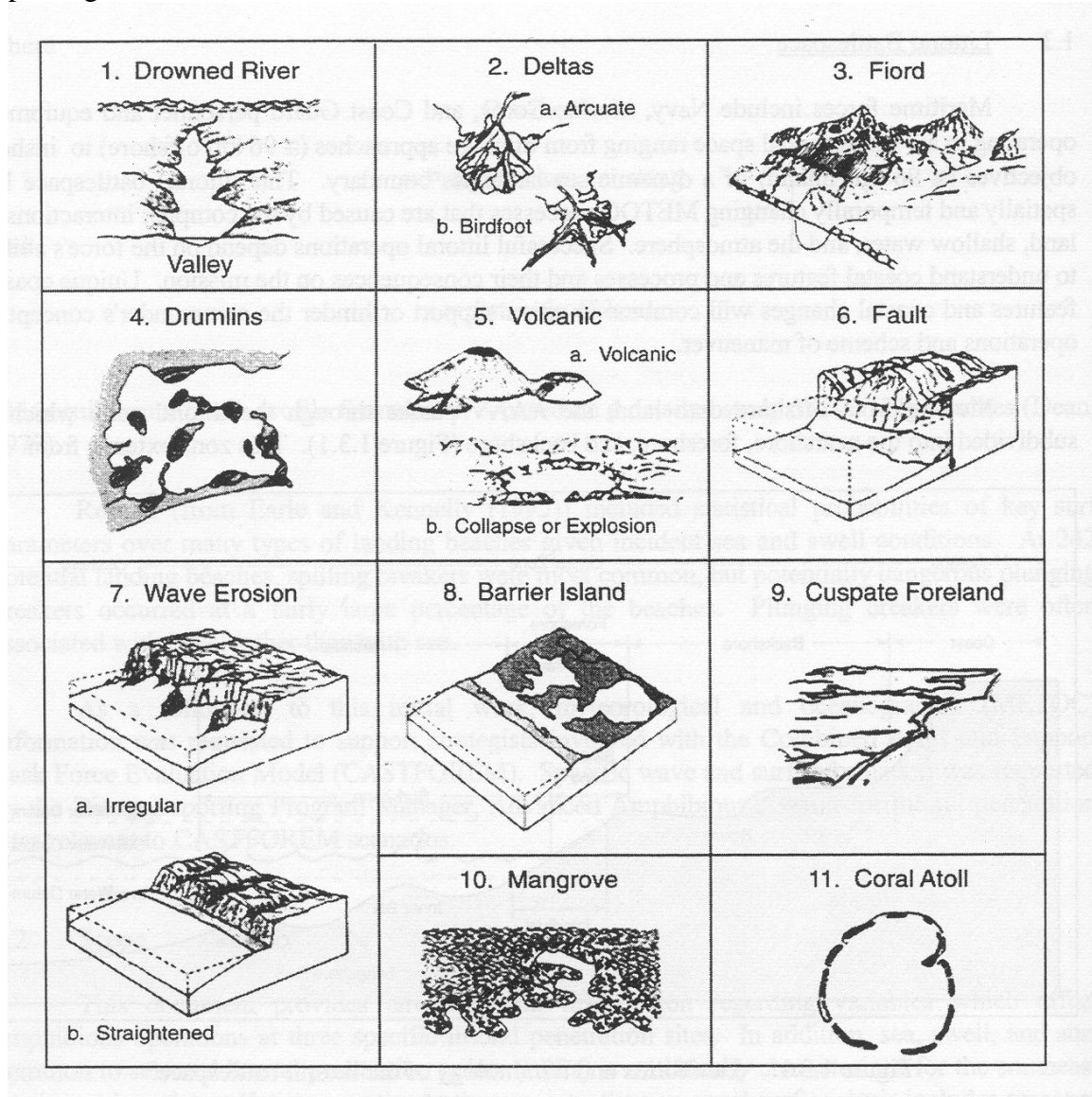
Figure E-1. Coastal Classifications. The interaction of physical and biological processes can form a variety of coastal types, each with unique consequences to naval expeditionary warfare.